Differential regulation of actin microfilaments by human MICAL proteins

Sai Srinivas Panapakkam Giridharan[1], Jennifer L. Rohn[2,*], Naava Naslavsky[1,*] and Steve Caplan[1,*]

[1]Department of Biochemistry and Molecular Biology and Eppley Cancer Center, University of Nebraska Medical Center, Omaha, Nebraska 68198-5870, USA
[2]MRC Laboratory for Molecular Cell Biology, University College London, London WC1E 6BT, UK
*Authors for correspondence (j.rohn@ucl.ac.uk; nnaslavsky@unmc.edu; scaplan@unmc.edu)

Accepted 26 September 2011
Journal of Cell Science 125, 614–624

doi: 10.1242/jcs.089367

Summary

The *Drosophila melanogaster* MICAL protein is essential for the neuronal growth cone machinery that functions through plexin- and semaphorin-mediated axonal signaling. *Drosophila* MICAL is also involved in regulating myofilament organization and synaptic structures, and serves as an actin disassembly factor downstream of plexin-mediated axonal repulsion. In mammalian cells there are three known isoforms, MICAL1, MICAL2 and MICAL3, as well as the MICAL-like proteins MICAL-L1 and MICAL-L2, but little is known of their function, and information comes almost exclusively from neural cells. In this study we show that in non-neural cells human MICALs are required for normal actin organization, and all three MICALs regulate actin stress fibers. Moreover, we provide evidence that the generation of reactive oxygen species by MICAL proteins is crucial for their actin-regulatory function. However, although MICAL1 is auto-inhibited by its C-terminal coiled-coil region, MICAL2 remains constitutively active and affects stress fibers. These data suggest differential but complementary roles for MICAL1 and MICAL2 in actin microfilament regulation.

Key words: MICAL1, MICAL2, Actin, Actin-rich protrusions, Microfilaments, Reactive oxygen species

Introduction

Actin plays a key role in maintaining cell shape, cell motility, chemotaxis and a multitude of crucial cellular functions including cytokinesis, signal transduction and endocytosis (Sutherland and Witke, 1999). Regulation of the axonal growth cone and the axonal guidance machinery is one such actin-regulated process that has been studied extensively over the past decade (Pak et al., 2008). Growth cones are highly motile sensory structures localized to the tip of the axons and essential for the guidance of neurons to their synaptic targets during embryonic development. Numerous soluble, matrix and cell-bound ligands mediate axonal guidance through binding to receptors at the tip of the axon or growth cone (Kalil and Dent, 2005). Upon binding to ligands, these receptors create localized changes in filamentous actin, which in turn modulate microtubule dynamics and thus induce changes in axonal direction.

Axons use both attractive and repulsive cues to accurately establish neuronal circuits. Semaphorins are one of the largest classes of guidance cues involved in axonal pathfinding, branching, fasciculation and neuronal polarity (He et al., 2002; Raper, 2000). Semaphorins bind to plexin receptors and modify the growth cone cytoskeleton to mediate repulsive signaling. Sema1A is a well-characterized transmembrane semaphorin involved in repulsive axonal guidance (Yu et al., 1998). When Sema1A binds to plexinA on neurons, this association promotes depolymerization of actin filaments. The mechanism of Sema1A-mediated axonal repulsion was clarified after the identification of MICAL (Molecules Interacting with CasL) in the fruit fly *Drosophila melanogaster* (Terman et al., 2002). *Drosophila* MICAL interacts with the cytoplasmic region of plexin and is required for pathfinding of motor axons.

Although MICAL was identified originally in mammals, its function has been studied primarily in *Drosophila*. *Drosophila* $MICAL^{-/-}$ flies displayed abnormally shaped bristles, whereas overexpression of MICAL in wild-type *Drosophila* caused the bristles to branch (Hung et al., 2010). Similar to neuronal extension by axonal guidance, the process of bristle elongation is also dependent on actin dynamics (Sutherland and Witke, 1999). Bristles of $MICAL^{-/-}$ flies had disorganized, intersecting and larger F-actin bundles, whereas in *Drosophila* overexpressing MICAL, bristles displayed a rearrangement of F-actin into a complex meshwork of short actin filaments (Hung et al., 2010). Moreover, MICAL directly induced actin depolymerization and significantly decreased the levels of actin filaments in vitro (Hung et al., 2010). These studies implicated MICAL as a direct effector of F-actin. Accordingly, *Drosophila* MICAL is likely to function downstream of semaphorin to cause actin destabilization and thus play an important role in repulsive axon guidance. Indeed, further evidence for this model is supplied by a study demonstrating that Sox14, a transcription factor necessary and sufficient to mediate dendrite severing, mediates dendrite pruning by directly regulating the expression of MICAL (Kirilly et al., 2009). *Drosophila* MICAL mutants also affect neuromuscular junctions, causing patterning and arrangement defects of synaptic boutons at the distal axonal termini (Beuchle et al., 2007).

Drosophila MICAL has been extensively studied; however, the roles of the mammalian MICAL proteins have not been well characterized. Human MICAL proteins have four conserved

domains: an N-terminal flavin adenine dinucleotide (FAD) binding domain, a calponin homology (CH) domain, a Lin11, Isl-1 and Mec-3 (LIM) domain and a C-terminal coiled-coil (CC) domain (Fig. 1A) (reviewed by Hung and Terman, 2011; Zhou et al., 2011a). MICAL1 has the most closely related domain architecture to *Drosophila* MICAL, whereas MICAL3 displays the least homology (Fig. 1B). Both MICAL1 and *Drosophila* MICAL have proline-rich regions that are required for binding to SH3 domains. However, unlike MICAL1, the CH and LIM domains of MICAL2 are separated by approximately 380 residues, and MICAL2 lacks a recognizable C-terminal CC domain.

It was demonstrated that both MICAL1 and MICAL2 interact with plexins (Terman et al., 2002), and that MICAL1 also interacts with collapsin response mediator proteins (CRMPs), which function downstream of plexin signaling (Schmidt et al., 2008). MICAL1, MICAL2 and MICAL3 are expressed in the embryonic postnatal and adult nervous systems, suggesting a role in neuronal growth cone machinery (Pasterkamp et al., 2006). These studies imply that mammalian MICALs could potentially function in actin remodeling, like *Drosophila* MICAL. To date, it remains unknown whether mammalian MICALs have any role apart from their function as neurite out-growth regulators. In particular, little is known about the expression and potential role(s) of human MICAL proteins in non-neuronal cells. In this study, we address the function of the human MICAL proteins that are expressed in non-neuronal cells, and provide evidence for a mechanism describing their differential regulation of actin microfilaments.

Results

To date, isolated studies have addressed the expression of MICAL proteins in neural cells, but even fewer studies have been performed in non-neural cells and tissues (Schmidt et al., 2008; Suzuki et al., 2002). We analyzed the expression of MICAL1 in a variety of both neural and non-neural cell lines, such as HeLa, retinal pigment epithelium (RPE), SKNMC neuroblastoma cells, squamous cell carcinoma (SCC), Caco-2 colon carcinoma cells, A431, LnCap prostate cancer cells and human foreskin fibroblast cells (Fig. 1C,D). As depicted, MICAL1 protein expression was detected in all of these cells. Moreover, the specificity of the

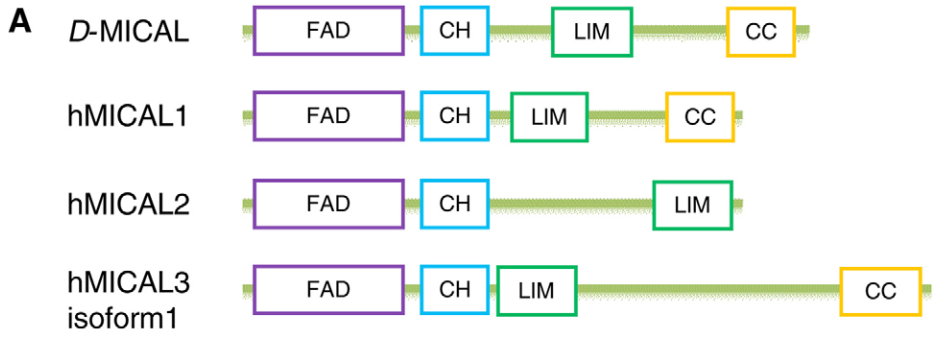

B

	D-MICAL / hMICAL1	*D*-MICAL / hMICAL2	*D*-MICAL / hMICAL3
Consensus	**35.4%**	**39.4%**	**22.1%**
Identity	**27.1%**	**30.5%**	**17.6%**

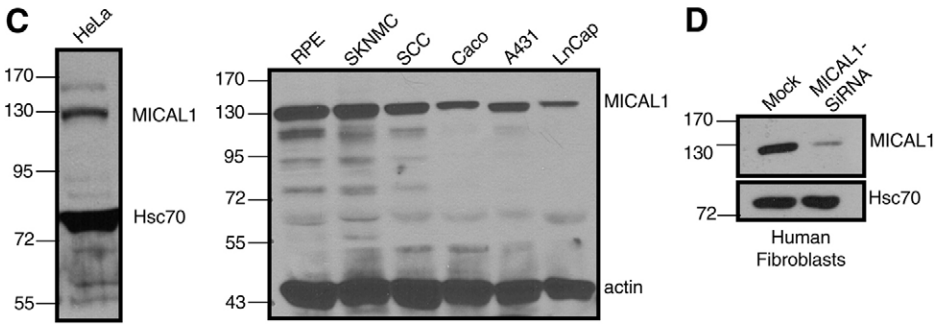

Fig. 1. MICAL1 is expressed in non-neuronal cell lines. (**A**) Domain architecture of *Drosophila* (*D*-)MICAL and human (h) MICAL1, MICAL2 and MICAL3 (isoform1). FAD, flavin-adenine-dinucleotide-binding domain; CH, calponin homology domain; LIM, Lin11, Isl-1, Mec-3 domain; CC, coiled-coil domain. (**B**) Amino acid sequence homology and identity between *D. melanogaster* MICAL (*D-MICAL*, isoform-A, NP_788627.1) and human MICALs (hMICAL1, NP_073602.3; hMICAL2, NP_055447.1; and hMICAL3 isoform1, NP_056056.2). (**C**) HeLa, retinal pigment epithelium (RPE), SKNMC, squamous cell carcinoma (SCC), Caco-2, A431 and LnCap cells were grown on 35-mm dishes, harvested, lysed and separated by SDS-PAGE. Proteins were transferred onto nitrocellulose membranes. Immunoblotting was performed with anti-MICAL1 antibody together with anti-β-actin or anti-Hsc70 antibodies. (**D**) Human fibroblasts grown on 35-mm dishes were either mock-treated or treated with siRNA against MICAL1 for 72 hours and lysed. Proteins were separated by SDS-PAGE, transferred to nitrocellulose membranes and immunoblotted with anti-MICAL1 and anti-Hsc70 antibodies.

MICAL1 antibodies could be verified by showing decreased MICAL1 immunoreactivity in MICAL1-depleted cells (Fig. 1D). On the other hand, utilizing both commercial antibodies and antisera generated in our laboratory, we were unable to detect MICAL2 or MICAL3 proteins in any of these cell lysates, although the antibodies we generated did recognize a band corresponding to overexpressed MICAL2 (our unpublished observations). To determine whether *MICAL2* and *MICAL3* mRNA is expressed in non-neural cells, we performed RT-PCR with several primers designed for MICAL2 and several isoforms of MICAL3. We found that *MICAL2* mRNA is indeed expressed in HeLa cells, as are mRNAs encoding MICAL1 and actin (supplementary material Fig. S1A). In addition, we could detect mRNAs for both MICAL3 isoform1 and MICAL3 isoform3 (supplementary material Fig. S1B). Previously, it was demonstrated that splice variants of MICAL2 were expressed in prostate cancer cells (Ashida et al., 2006). By designing various primers against the different regions of MICAL2 we were able to verify the isoform that is expressed in HeLa cells, namely that corresponding to accession number NM_014632.2.

Because overexpression of MICAL in *Drosophila* caused the normal, parallel organization of bundled F-actin in the bristles into a complex meshwork of short actin filaments (Hung et al., 2010), we hypothesized that expression of exogenous MICALs in mammalian cells might influence actin organization. Accordingly, we began by transfecting hemagglutinin (HA)-tagged MICAL2 into HeLa cells (Fig. 2A–C). The exogenous MICAL2 localized to the plasma membrane, and its expression correlated with the loss of actin stress fibers as well as a concentration of actin in filopodia-like protrusions at the cell periphery (Fig. 2A–C and quantified in 2P; arrows denote actin at the cell periphery in actin-rich protrusions).

To delineate the domain(s) responsible for actin rearrangement, we performed a series of truncations (Fig. 2D–O). Removal of either the C-terminal LIM domain (Fig. 2D–F) or the LIM domain along with the linker region between the LIM and CH domains (Fig. 2G–I) did not prevent actin stress fiber loss upon transfection into cells. Moreover, we observed that the MICAL2 FAD domain is both required and sufficient for actin stress fiber loss (Fig. 2J–L). Instituting conserved glycine

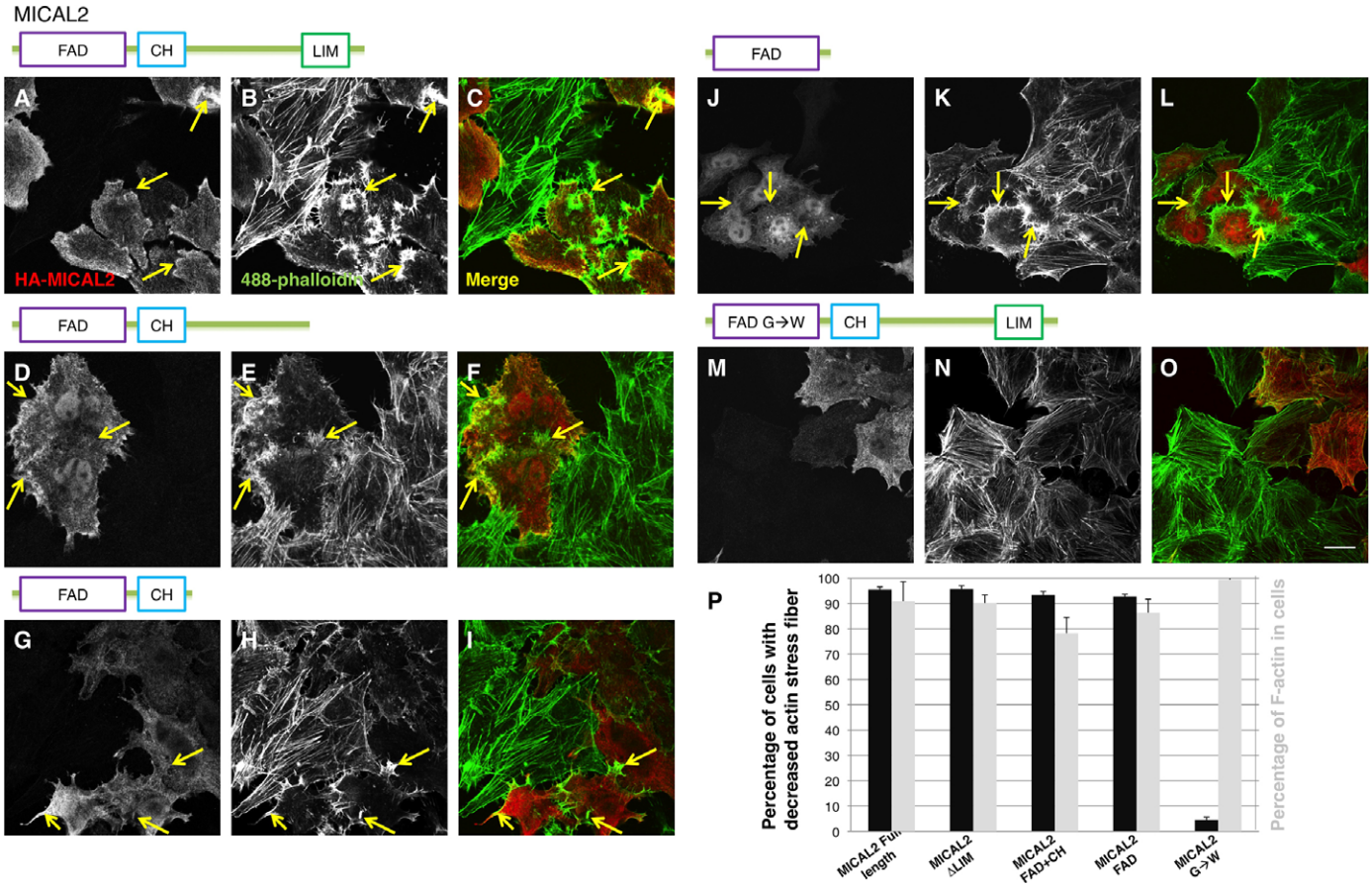

Fig. 2. MICAL2 expression induces loss of actin stress fibers and the generation of actin-rich protrusions. (**A**–**O**) HeLa cells grown on coverslips were transiently transfected with either full-length HA–MICAL2 (A–C), truncated HA–MICAL2 (residues 1–987) lacking the LIM domain (D–F), truncated HA–MICAL2 (residues 1–631) containing the FAD and CH domains (G–I), truncated HA–MICAL2 (residues 1–499) containing only the FAD domain (J–L), or full-length HA–MICAL2 with residues 91–96 (GGGPCG) mutated to WAWPCW (M–O). After 18 hours, cells were fixed, permeabilized and incubated with anti-HA antibody followed by Alexa-Fluor-568-conjugated anti-mouse secondary antibody and Alexa-Fluor-488-conjugated phalloidin. Arrows indicate filopodial actin outgrowth in MICAL2-transfected cells. Scale bar: 10 μm. (**P**) Quantification of the effects described in A–O. A minimum of 100 transfected cells for each tranfection were used to count the percentage of cells displaying a decreased number of actin stress fibers (cells displaying fewer than five prominent stress fibers) compared with untransfected cells. F-actin levels were quantified from a minimum of 30 untransfected and transfected cells from each transfection of each MICAL construct. Quantification was performed using LSM5 Pascal software with data derived from three independent experiments. Error bars indicate s.e.m.

to tryptophan point mutations within the *Drosophila* MICAL FAD domain was previously shown to impair FAD binding and enzymatic activity (Terman et al., 2002). When a similar mutation was generated in the FAD domain of MICAL2, expression of this mutant FAD domain failed to induce the loss of actin stress fibers (Fig. 2M–O). The percentage of cells transfected with HA–MICAL2 that displayed loss of identifiable actin stress fibers (compared with 100% for untransfected control cells) was quantified for HA–MICAL2 and the MICAL2 mutants (Fig. 2P). In addition, quantification was carried out to calculate the percentage of F-actin in the transfected cells compared with untransfected cells (Fig. 2P). As observed, although several mutants displayed mild reductions in overall F-actin levels (for example, MICAL2 FAD + CH domains was ~80% compared with 100% in untransfected cells), these differences were relatively minor compared with the massive numbers of transfected cells displaying loss of stress fibers.

Unlike MICAL2, wild-type MICAL1 overexpression had no discernable effect on F-actin stress fiber loss or total F-actin compared with untransfected cells (Fig. 3A–C; quantified in Fig. 3S). Indeed, unlike MICAL2, the overexpressed MICAL1 was largely cytoplasmic in its distribution. Surprisingly, truncation of the C-terminal MICAL1 CC region led to a dramatic reduction in the percentage of cells exhibiting actin stress fibers as well as decreased levels of overall F-actin when overexpressed (Fig. 3D–L; quantified in Fig. 3S). Unexpectedly, in the absence of the last 268 amino acids (including the CC), MICAL1 exhibited a partial nuclear localization (Fig. 3D). Although the reason for this remains unclear, this mutant was nonetheless capable of inducing a considerable decrease in the percentage of cells displaying stress fibers along with a decrease in total F-actin (Fig. 3D–F; quantified in Fig. 3S). Expression of MICAL1 with a truncation prior to the LIM domain (MICAL1 FAD+CH) again resulted in a cytoplasmic distribution of the mutant protein, and similarly resulted in a radical decrease in the percentage of cells with actin stress fibers and the amount of total F-actin per cell (Fig. 3G–I; quantified in Fig. 3S). As demonstrated for MICAL2, expression of an active MICAL1 FAD domain was both required and sufficient for loss of stress fibers and decreased total actin, as indicated by the dramatic loss of microfilaments induced by MICAL1 FAD expression (Fig. 3J–L; quantified in Fig. 3S). Moreover MICAL1 FAD-transfected cells also displayed a decrease in the number of focal adhesion plaques (supplementary material Fig. S2). Similar to our results with MICAL2, a mutant predicted to display impaired FAD binding and reduced enzymatic activity prevented stress fiber loss and F-actin depletion (Fig. 3M–O; quantified in Fig. 3S).

Given that the presence of the MICAL1 CC domain appeared to be crucial for the prevention of stress fiber loss upon MICAL1 overexpression, we hypothesized that expression of a MICAL1 mutant with a mutated CC might lead to stress fiber loss, as observed with wild-type MICAL2 expression. As demonstrated by the Paircoil algorithm in supplementary material Fig. S3 (http://groups.csail.mit.edu/cb/paircoil/cgi-bin/paircoil.cgi), replacement of alanines 940 and 941 with proline residues was predicted to interfere with generation of the CC. Indeed, overexpression of this mutant revealed that in the absence of a functional CC, MICAL1 expression induced a loss of actin stress fibers and decreased the cellular F-actin levels (Fig. 3P–R; quantified in Fig. 3S). These data suggest that MICAL2 constitutively controls stress fibers via its FAD domain, whereas the MICAL1 FAD domain is normally inhibited via its CC domain.

Next, we directly addressed the hypothesis that the MICAL1 protein is functionally different from the constitutively active *Drosophila* MICAL and MICAL2 due to the presence of its inhibitory CC domain. For this, we constructed a pair of chimeric proteins: the N-terminal MICAL1 FAD and CH domains followed by the central region and LIM domain of MICAL2 (MICAL1/MICAL2), and the MICAL2 FAD and CH domains fused to the LIM and CH domains of MICAL1 (MICAL2/MICAL1) (Fig. 4A). In cells expressing HA–MICAL1/MICAL2, we observed a decrease in the number of stress fibers and the appearance of actin-rich protrusions (Fig. 4B–D; see outlined cells, insets and arrows). However, cells expressing HA–MICAL2/MICAL1 did not display decreased levels of actin stress fibers (Fig. 4E–G). At lower expression levels, HA–MICAL2/MICAL1 partially localized to filamentous structures that displayed minimal colocalization with F-actin (supplementary material Fig. S4). These results support the idea that the FAD domains of MICAL1 and MICAL2 are both potent actin stress fiber regulators, and that the MICAL1 CC region is responsible for an auto-inhibitory mechanism that prevents FAD function, the depletion of stress fibers and the formation of actin-rich structures at the cell periphery.

Given the dramatic effects of MICAL2 and MICAL1 FAD overexpression on actin stress fibers, we carried out a series of studies to determine whether expression of these proteins had more widespread effects on the cells. As demonstrated in supplementary material Fig. S5, despite the potent effects on stress fibers, these proteins had little effect on early endosomes (EEA1; supplementary material Fig. S5A), the Golgi (Giantin; supplementary material Fig. S5B), and lysosomes (our unpublished observations). We did observe some reorientation of α-tubulin to actin-rich structures upon high levels of HA–MICAL1 FAD overexpression (supplementary material Fig. S5C), as well as centralization of γ-tubulin in HA–MICAL1 FAD-transfected cells (supplementary material Fig. S5D). However, little change was observed for Arp-3, myosin Vb or myosin Vc (our unpublished observations) upon transfection of either HA–MICAL2 or the MICAL1 FAD domain, indicating that the effects are highly specific for actin stress fibers and that there is little impact on endocytic organelles, actin nucleation via the ARP2/3 complex, and actin motors.

Studies on *Drosophila* MICAL indicate that its depletion affects actin architecture and bristle morphology (Hung et al., 2010). Accordingly, we next assessed the effect of MICAL1 and MICAL2 depletion on cellular F-actin. As demonstrated, RNA interference (RNAi) was successful in depleting >90% of endogenous MICAL1 (Fig. 5D) and >70% of exogenously expressed MICAL2 (Fig. 5E). In contrast to mock-treated cells (Fig. 5A), those lacking either MICAL1 or MICAL2 displayed radically altered F-actin morphology, with the loss of prominent stress fibers, enhanced levels of cortical actin, an enrichment of actin puncta in the cytoplasm, and F-actin concentrated in actin-rich protrusions (Fig. 5B,C; quantified in Fig. 6E). In addition, depletion of MICAL3 (as reflected by loss of mRNA for the MICAL3 isoform3 and modestly decreased expression of the MICAL3 isoform1; supplementary material Fig. S1B) induced enhanced levels of stress fibers per cell, and more elongated cells were observed (supplementary material Fig. S6). These results

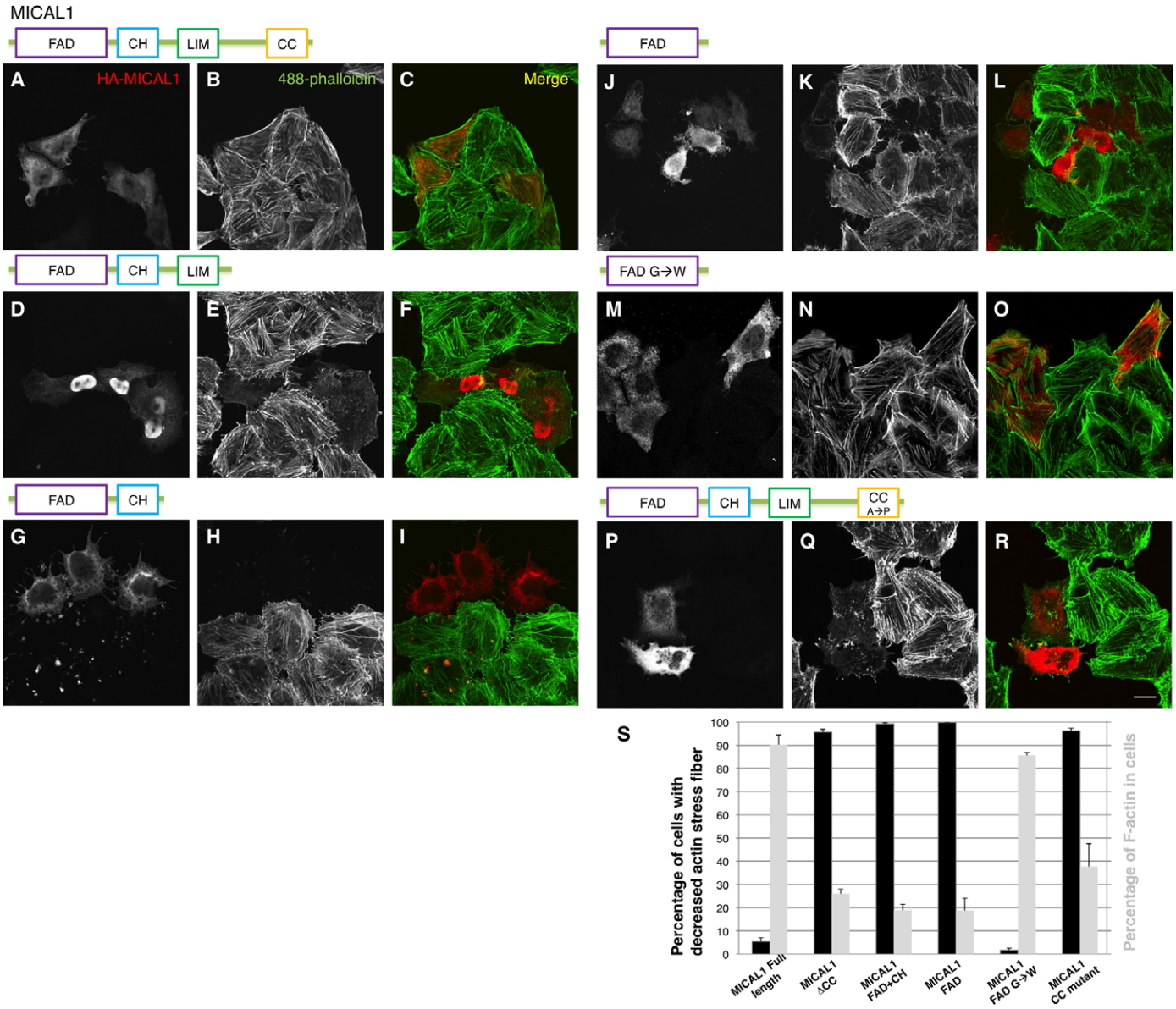

Fig. 3. MICAL1 differs from MICAL2 and does not constitutively induce loss of actin stress fibers. (**A–R**) HeLa cells grown on coverslips were transiently transfected with either full-length HA–MICAL1 (A–C), truncated HA–MICAL1 (residues 1–799) lacking the CC domain (D–F), truncated HA–MICAL1 (residues 1–621) containing the FAD and CH domains (G–I), truncated HA–MICAL1 (residues 1–499) containing only the FAD domain (J–L), truncated HA–MICAL1 containing only the FAD domain but with residues 91–96 (GAGPCG) mutated to WAWPCW (M–O), or full-length HA–MICAL1 with residues 940–941 (AA) mutated to PP (P–R). After 18 hours, the cells were fixed, permeabilized and incubated with anti-HA antibody followed by Alexa-Fluor-568-conjugated anti-mouse secondary antibody and Alexa-Fluor-488-conjugated phalloidin. Scale bar: 10 μm. (**S**) Quantification of the effects described in A–R. A minimum of 100 transfected cells for each tranfection were used to calculate the percentage of cells displaying a decreased number of actin stress fibers (cells displaying fewer than five prominent stress fibers) compared with untransfected cells. F-actin levels were quantified from a minimum of 30 untransfected and transfected cells from each transfection of each MICAL construct. Quantification was performed using LSM5 Pascal software with data derived from three independent experiments. Error bars indicate s.e.m.

indicate that mammalian MICALs play an important role in the organization of actin stress fibers.

To verify that the effects of MICAL protein knockdown are directly related to the loss of protein expression (and are not off-target effects), we instituted a ‘rescue’ system in which siRNA-resistant MICAL1 (with silent mutations in the cDNA) was reintroduced into depleted cells. As demonstrated (Fig. 6), the expression of HA–MICAL1 could be efficiently depleted with siRNA, and a siRNA-resistant HA–MICAL1 could be expressed in siRNA-treated cells (Fig. 6A,D). Moreover, cells expressing the siRNA-resistant HA–MICAL1 showed a decrease in actin-rich protrusions compared with the non-transfected (but MICAL1-depleted) cells (Fig. 6A–C; see non-transfected cells within dashed red lines and yellow arrows depicting protrusions). Because the generation of actin-rich protrusions was the most dramatic phenotype in MICAL1 knockdown cells, we used the presence of these structures to quantify the effects of knockdown of MICAL1 and MICAL2, as well as the ‘rescue’ of MICAL1 knockdown

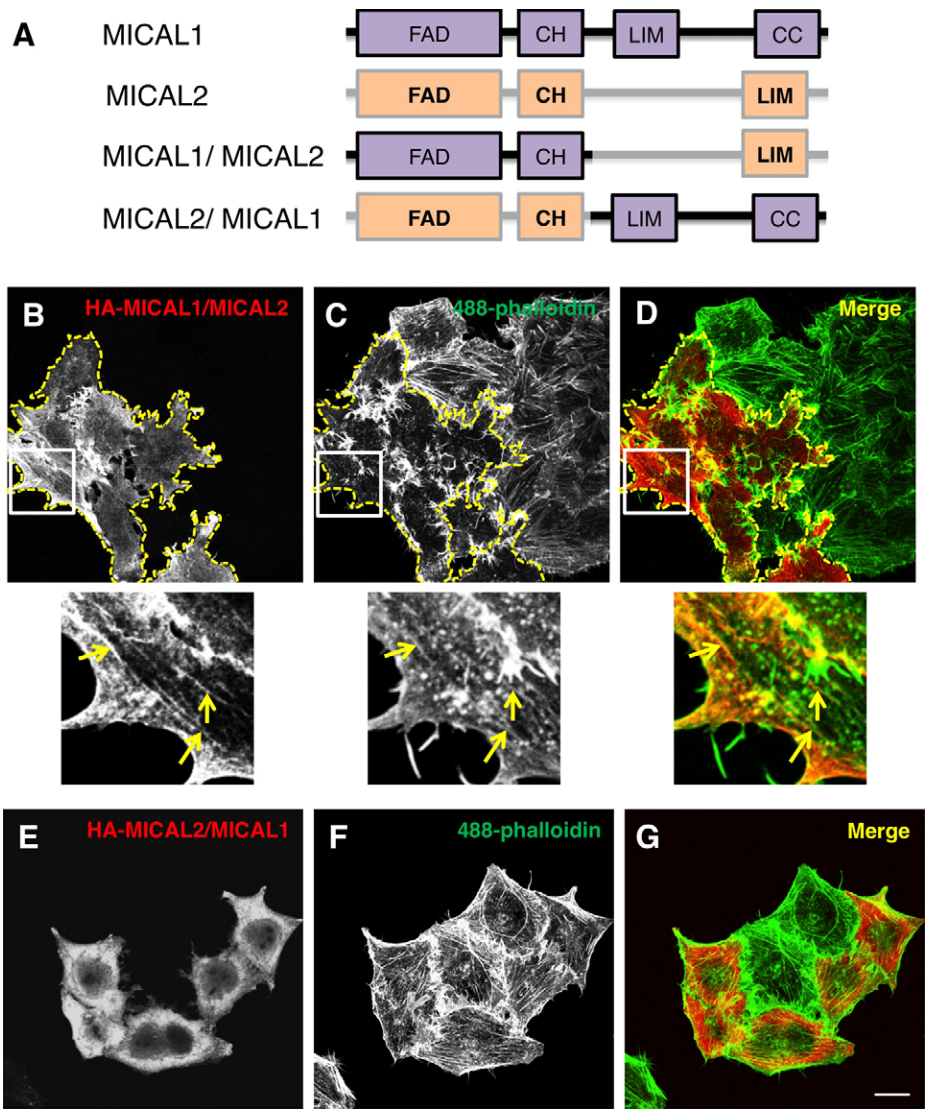

Fig. 4. The MICAL1 C-terminal region regulates its activity. (**A**) Domain architecture of wild-type MICAL1, wild-type MICAL2 and chimeras MICAL1–MICAL2 (MICAL1/MICAL2) and MICAL2–MICAL1 (MICAL2/MICAL1). (**B**–**G**) HeLa cells on coverslips were transiently transfected with either HA–MICAL1/MICAL2 (B–D) or HA–MICAL1/MICAL2 (E–G). After 18 hours, cells were fixed, permeabilized and incubated with anti-HA antibody followed by Alexa-Fluor-568-conjugated anti-mouse secondary antibody and Alexa-Fluor-488-conjugated phalloidin. Dotted lines depict transfected cells. Insets and arrows show partial colocalization of the MICAL1–MICAL2 chimera with actin microfilaments. Scale bar: 10 μm.

(Fig. 6E). As demonstrated, less than 15% of untreated cells normally displayed actin-rich protrusions, but knockdown of MICAL1 or MICAL2 increased the percentage of cells containing actin-rich protrusions to about 90% and 80%, respectively (Fig. 6E). Reintroduction of MICAL1 partially 'rescued' the knockdown phenotype, with only 50% of the cells exhibiting actin-rich protrusions (compared with >90% for MICAL1 knockdown). Because both MICAL2 knockdown and overexpression have complex effects on cellular actin, we were unable to carry out similar quantifiable rescue studies with this paralog.

Recent studies have shown that the MICAL1 FAD has the ability to produce H_2O_2 in vitro, and it has been proposed that generation of reactive oxygen species (ROS) might be an essential mechanism by which MICAL induces F-actin reorganization (Nadella et al., 2005; Schmidt et al., 2008). To determine whether the MICAL1 FAD domain is capable of inducing ROS generation, we used dihydrocalcein to detect ROS in HeLa cells expressing various MICAL constructs. Without transfection, very few cells contained detectable ROS levels (Fig. 7A). In cells expressing wild-type MICAL1, which does not induce loss of F-actin or actin-rich protrusions, ROS levels remained low (Fig. 7B,C and quantified in 7J). Cells transfected with the FAD domain (only) from MICAL1 displayed tenfold higher ROS levels (Fig. 7D,E and quantified in 7J). However, upon transfection of the enzymatically impaired MICAL1 FAD domain mutant (glycine to tryptophan point mutations), the levels of ROS were only slightly higher than the baseline levels observed upon MICAL1 expression (Fig. 7F,G and quantified in 7J). By contrast, MICAL2 expression induced three- to fourfold higher levels of ROS than did MICAL1 expression (Fig. 7H,I and quantified in 7J). To determine whether individual cells expressing the active MICAL1 FAD domain exhibited higher levels of ROS, we overexpressed Tomato-tagged MICAL1 FAD in HeLa cells treated with the fluorescent dye H_2DCFDA (supplementary material Fig. S7). First, we showed that expression of Tomato–MICAL1-FAD had similar effects to HA–MICAL1-FAD, causing loss of actin stress fibers and the generation of actin-rich protrusions (supplementary material Fig. S7A–C). To detect levels of ROS in individual transfected cells, we imaged fields of cells transfected with either Tomato alone (supplementary material Fig. S7D–F; control), or Tomato–MICAL1-FAD (supplementary material Fig. S7G–I). As demonstrated, expression of the Tomato protein had no effect on the levels of ROS produced in the cells (supplementary

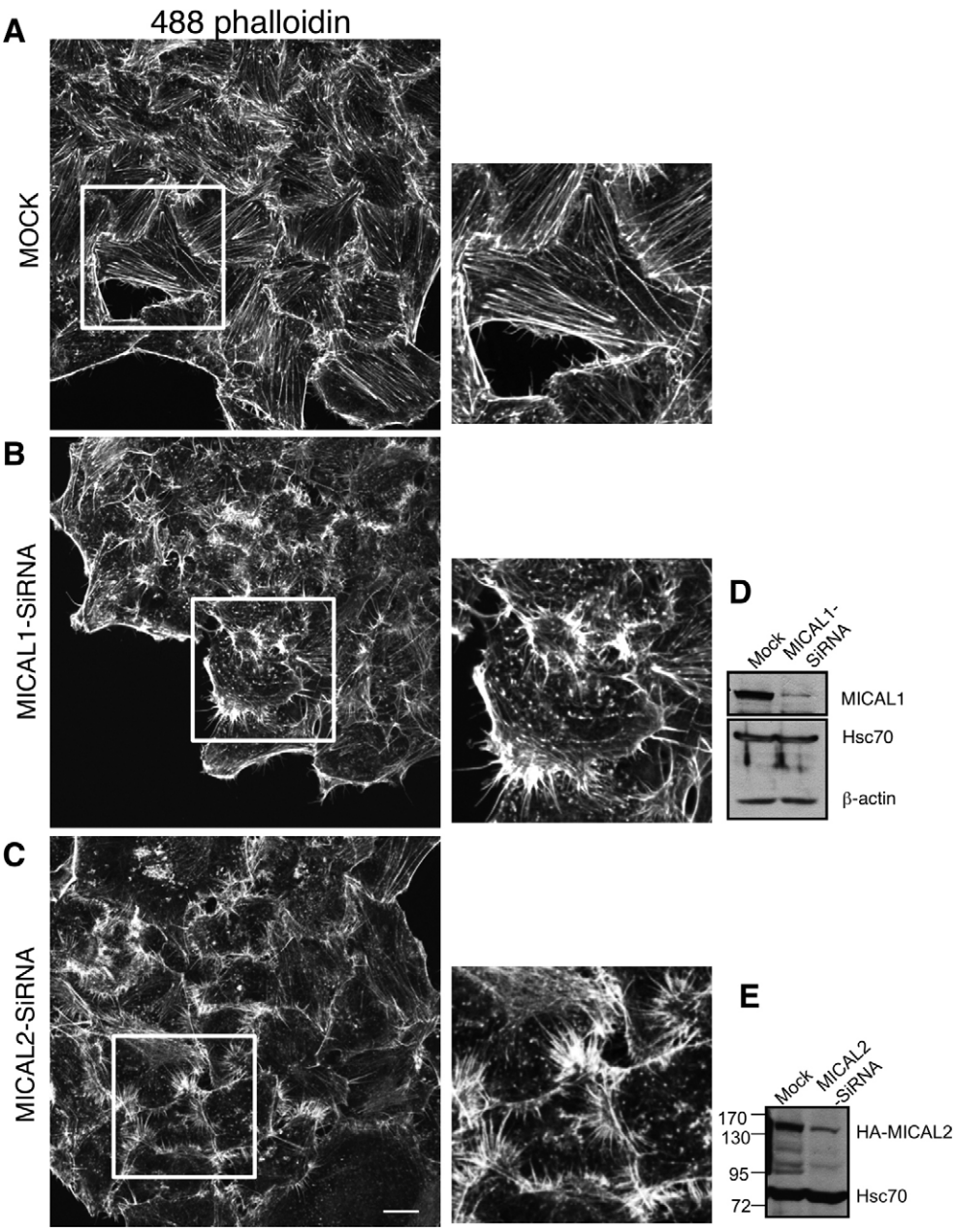

Fig. 5. Depletion of either MICAL1 or MICAL2 induces the generation of actin-rich protrusions. (**A**–**C**) HeLa cells grown on coverslips were either mock-treated (A), treated with siRNA against MICAL1 (B) or with siRNA against MICAL2 (C). After 72 hours, cells were fixed, permeabilized and incubated with Alexa-Fluor-488-conjugated phalloidin. Scale bar: 10 µm. Magnifications of boxed areas are shown on the right. (**D**) HeLa cells grown on 35-mm dishes were either mock-treated or treated with siRNA against MICAL1 for 72 hours and lysed. Proteins were separated by SDS-PAGE, transferred to nitrocellulose membranes and immunoblotted with anti-MICAL1, anti-Hsc70 and anti-β-actin antibodies. (**E**) HeLa cells grown on 35-mm dishes were either mock-treated or treated with siRNA against MICAL2 for 72 hours. In addition, cells were transfected with HA-tagged MICAL2 for the last 48 hours of the treatment. The cells were then lysed, proteins were separated by SDS-PAGE and transferred to nitrocellulose membranes. Immunoblotting was performed with anti-HA and anti-Hsc70 antibodies.

material Fig. S7D–F). On the other hand, cells expressing the Tomato-tagged FAD induced high levels of ROS in transfected cells (supplementary material Fig. S7G–I). Overall, these results lend credence to the notion that MICAL proteins exert their effects on actin microfilaments, at least in part, through the generation of ROS via their FAD domains.

Discussion

Although *Drosophila* MICAL and its role in growth cone repulsion has been well studied over the years, relatively little is known about its mammalian counterparts, especially in the context of non-neural cells. Human MICAL1 was originally identified as an interaction partner for CasL and vimentin (Suzuki et al., 2002) and later as a Rab1 interaction partner (Weide et al., 2003). Other studies determined that MICAL1 functions in tandem with CRMP2 to regulate the semaphorin–plexin signaling pathway (Schmidt et al., 2008). MICAL1, whose monooxygenase domain-mediated NADPH oxidation is stimulated by F-actin (Zucchini et al., 2011), was also recently described as an interaction partner and negative regulator of nuclear Dbf2-related (NDR) kinases and thus impacts apoptosis (Zhou et al., 2011b). MICAL2, on the other hand, has a number of splice variants that are expressed in prostate cancer cells (Ashida et al., 2006), whereas MICAL3 has functions downstream of the semaphorin pathway in motor neurons (Bron et al., 2007). A very recent report shows that MICAL3 interacts with both Rab8 and ELKS, linking exocytic vesicles to the plasma membrane, and that its monooxygenase activity is required for exocytic activity (Grigoriev et al., 2011). Studies with rat models have led to the conclusion that MICAL proteins are expressed in embryonic, postnatal and adult nervous systems (Pasterkamp et al., 2006). Although most of these studies highlight the roles of mammalian

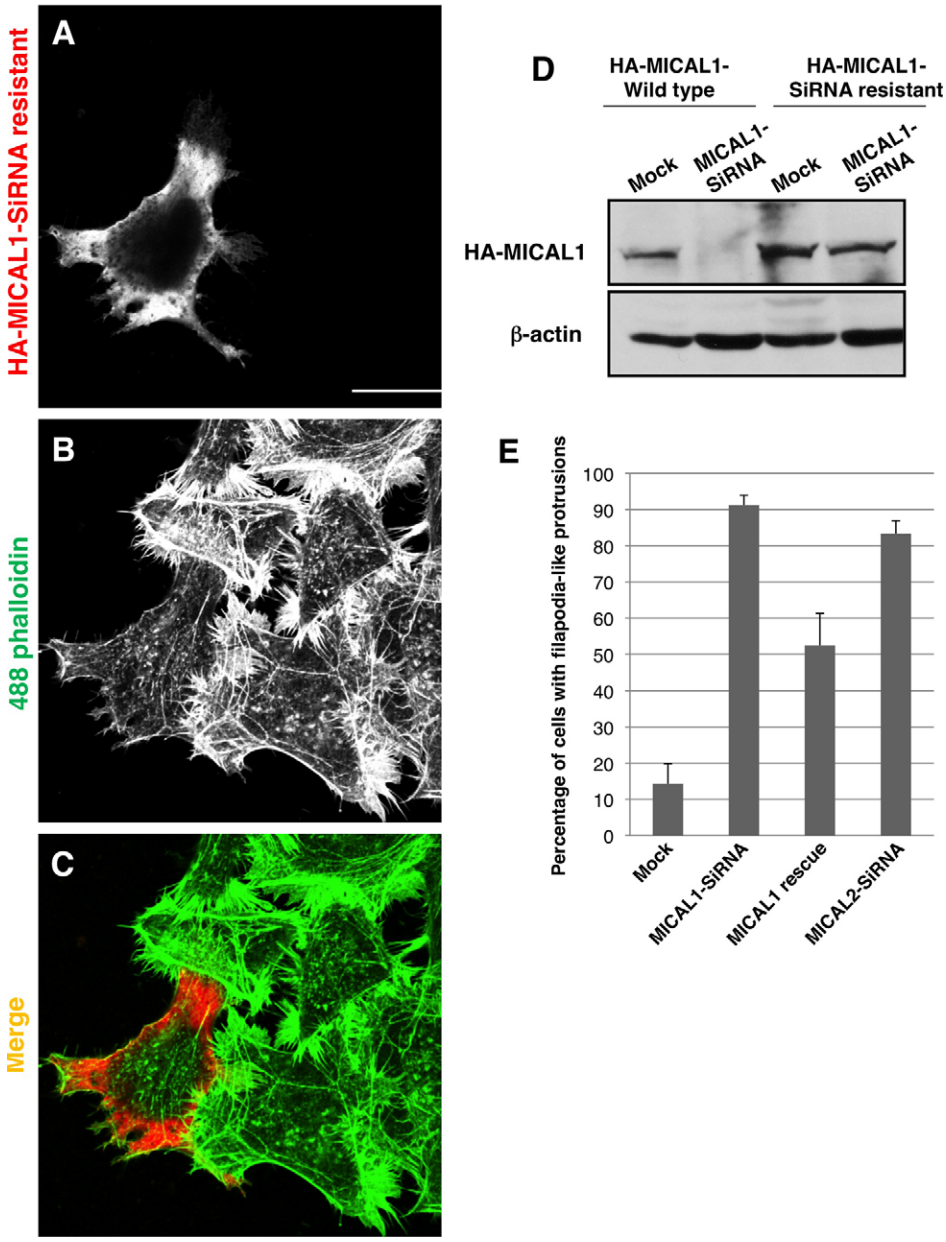

Fig. 6. Partial rescue of the actin-rich protrusions induced by MICAL1 depletion upon reintroduction of an siRNA-resistant *MICAL1* cDNA. (**A–C**) HeLa cells grown on coverslips were treated with siRNA against MICAL1 for 72 hours. The cells were transiently transfected with a HA–MICAL1 siRNA-resistant construct for the last 48 hours of treatment. Cells were then fixed, permeabilized and incubated with anti-HA antibody followed by Alexa-Fluor-568-conjugated anti-mouse secondary antibody and Alexa-Fluor-488-conjugated phalloidin. Scale bar: 10 μm. (**D**) HeLa cells grown on 35-mm dishes were either mock-treated or treated with siRNA against MICAL1 for 72 hours. Cells were transfected with either wild-type HA–MICAL1 or siRNA-resistant HA–MICAL1 constructs for the last 48 hours of treatment. The cells were then lysed, proteins were separated by SDS-PAGE and transferred to nitrocellulose membranes. Immunoblotting was performed with anti-HA and anti-β-actin antibodies. (**E**) HeLa cells grown on coverslips were either mock-treated or treated with siRNAs against MICAL1 or MICAL2 for 72 hours. Cells treated with siRNA against MICAL1 were either untransfected or transfected with a HA–MICAL1 siRNA-resistant construct (MICAL1 rescue) for the last 48 hours. HeLa cells displaying filapodial-like protrusions in these treatments were quantified from three independent experiments. Quantifications were performed with a minimum of 80 cells per treatment, and three independent experiments were performed. Error bars indicate s.e.m.

MICAL proteins in development and in neural cells, the precise functions of these proteins in non-neural cells have remained largely unanswered.

Here, we have functionally compared mammalian MICALs using HeLa cells as a non-neural model system and have shown that MICAL1 and MICAL2 are both expressed at the RNA level. Various isoforms of MICAL3 are also expressed in HeLA cells, but we chose here to focus on MICAL1 and MICAL2, which are more closely related at the sequence level to *Drosophila* MICAL. Although the human MICAL-like proteins MICAL-L1 and MICAL-L2 play important roles in endocytic regulation (Sharma et al., 2009; Terai et al., 2006), we found that the human MICALs had no detectable effects on endocytic organelles and actin motor proteins. Consistent with *Drosophila* MICAL, human MICALs had only modest effects on α- and γ-tubulin localization. Instead, our various studies taken together suggest that the human MICALs play a key role in actin organization in non-neural cells. In particular, overexpression and domain-swapping studies point to the MICAL FAD domain as being crucial for actin-based structures. Specifically, overexpression of a MICAL2 construct, or of an intact FAD domain, led to a dramatic dismantling of actin stress fibers and a concomitant increase in actin-rich filopodia- or microspike-like protrusions. Because this was accompanied without an overall change in F-actin levels, we propose that enhanced MICAL2 expression could lead to a repurposing of cellular actin from stress fibers to protrusions.

By contrast, overexpression of wild-type MICAL1 had no effect on actin structures. However, domain experiments showed that this lack of phenotype was due to the presence of an autoinhibitory CC domain, because removal of this region led to a dramatic decrease in stress fibers, consistent with observations upon MICAL2 overexpression. As with MICAL2, an intact MICAL1 FAD domain was necessary and sufficient to

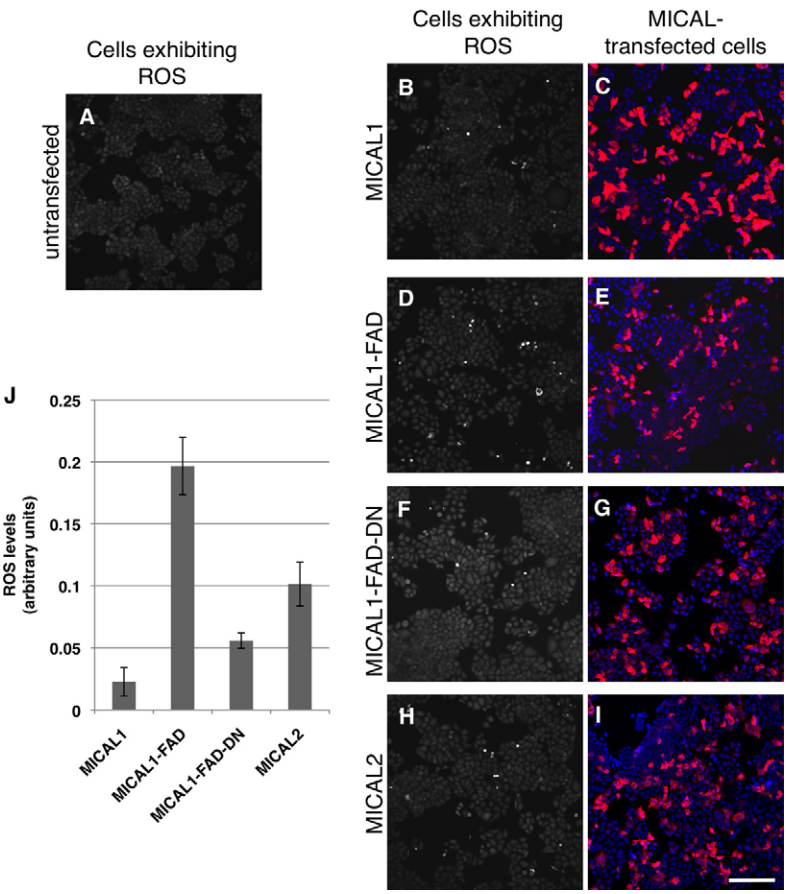

Fig. 7. Self-inhibitory MICAL1 is unable to generate ROS. (**A**–**I**) HeLa cells grown on coverslips were either untreated (A) or transiently transfected with wild-type HA–MICAL1 (B,C), HA-tagged MICAL1 FAD domain only (D,E), HA-tagged MICAL1 FAD domain with residues 91–96 (GAGPCG) mutated to WAWPCW (F,G), or wild-type HA–MICAL2 (H,I). After 18 hours, cells were either treated with dihydrocalcein (A,B,D,F,H) and analyzed or fixed (C,E,G,I). Fixed cells were permeabilized and incubated with anti-HA antibody, followed by Alexa-Fluor-568-conjugated anti-mouse secondary antibody. Cells were then mounted in solution containing DAPI. Scale bar: 100 μm. (**J**). Quantification of ROS levels in the transfected cells shown in B–I. Error bars indicate s.e.m.

recapitulate the uninhibited phenotype. Unlike MICAL2 overexpression, however, this shift in actin organization was accompanied by a decrease in overall F-actin levels, which highlights the fact that these two proteins, once activated, have subtly different functions. Indeed, domain-swapping experiments confirmed that the specific effect on actin could be mapped to the FAD domain, and that the autoinhibitory domain resides in the CC domain of MICAL1.

How do these results compare to our current understanding of *Drosophila* MICAL? Overexpression of *Drosophila* MICAL in bristles caused the F-actin to rearrange and form a complex meshwork of short filaments (Hung et al., 2010). Although these and other studies have also implicated *Drosophila* MICAL function in the disassembly of F-actin bundles and filaments, we have found important differences between *Drosophila* MICAL and human MICAL function. For example, unlike its human counterparts, *Drosophila* MICAL requires its CH as well as its FAD domain to be functionally active. Another key difference that we observed was in the subcellular localization of the proteins. For example, *Drosophila* MICAL is reported to be a cytoplasmic protein (Terman et al., 2002) and MICAL1 similarly displayed a cytoplasmic distribution, but MICAL2 was mostly localized proximal to the plasma membrane. This shows that the biology of mammalian MICALs, perhaps not surprisingly, might be more complicated than in the simpler *Drosophila* system. Because MICAL2, like *Drosophila* MICAL, is not autoinhibited, and because MICAL2 shows the highest protein sequence identity with *Drosophila* MICAL, MICAL2 might be functionally more similar to *Drosophila* MICAL than is MICAL1. Future studies to clarify the 'true' *Drosophila* MICAL ortholog might include rescue experiments using MICAL1 and MICAL2 in $MICAL^{-/-}$ flies and testing whether the human MICALs are able to rescue the bristle morphology defects.

In this study, we found that stress fiber loss mediated by the MICAL FAD domain is accompanied by the production of ROS. Previous studies have demonstrated the ability of the MICAL1 FAD domain to generate ROS in vitro (Hung et al., 2010; Nadella et al., 2005; Schmidt et al., 2008). ROS have the ability to modify cysteine, methionine and tryptophan residues of actin, which might cause structural changes, the inability of actin to polymerize and its potential degradation (Dalle-Donne et al., 2002; Fedorova et al., 2010). Moreover, upon activation by its coenzyme NADPH, *Drosophila* MICAL causes a decrease in steady-state levels of actin polymerization (Hung et al., 2010). In addition, given that *Drosophila* MICAL does not destabilize actin by acting as a sequestering or capping protein, and that it decreases the rate and extent of actin polymerization (reviewed by Hung and Terman, 2011), the in vitro studies by Hung and co-workers suggest that *Drosophila* MICAL acts directly on actin through ROS production (Hung et al., 2010). However, until that study it had not been determined whether ROS are actually generated by MICAL proteins in cells (reviewed by Kolk and Pasterkamp, 2007).

Initially, we verified the ability of the MICAL1 FAD domain to produce ROS in vivo. It was previously determined that the anti-oxidant (-) epigallocatechin gallate (EGCG) can act as a pharmacological inhibitor of *Drosophila* MICAL monooxygenase

activity in vivo (Terman et al., 2002). However, EGCG could potentially function either in monooxygenase inhibition, or more indirectly by suppressing MICAL-induced ROS. We found that a general antioxidant, *N*-acetyl cysteine (NAC), partially rescues stress fiber levels upon MICAL1 FAD domain overexpression (our unpublished observations). On the other hand, the MICAL2 FAD caused actin-rich protrusions, but not a loss of total F-actin (as observed for MICAL1). These studies are complicated, however, by the effects that NAC itself has on the actin cytoskeleton, and are thus difficult to interpret. However, the demonstration that individual cells transfected with an active FAD domain display both stress fiber loss as well as high levels of ROS is highly suggestive. It is likely that MICAL proteins, at least in part, affect actin microfilaments through their ability to produce ROS.

How might MICAL-induced ROS regulate F-actin structures? It is of interest that Rac1 has been implicated in depolymerization of actin microfilaments via ROS production (Moldovan et al., 1999). Also, Nimnual and colleagues reported that Rac suppresses Rho activity via this ability to generate ROS (Nimnual et al., 2003). Given that Rho dampening is associated with the dismantling of stress fibers (Ridley and Hall, 1992), it is possible that ROS generated by MICAL1 could feed into this same pathway and explain the similar phenotype we have observed. Regardless, because both Rac and MICAL proteins can function downstream of plexin, it remains to be determined whether Rac affects MICAL function or vice versa. It would also be interesting to see whether actin residues are modified by MICAL1 and/or MICAL2; potential differences in amino acid modifications might help explain why MICAL1 causes complete stress fiber depletion but MICAL2 primarily induces actin-rich protrusions. In addition, there is at least precedence for mammalian MICALs affecting actin structures other than stress fibers. For example, a previous study demonstrated that overexpression of the MICAL1 FAD domain induces a reduction in cell area via a retraction of the lamellipodia, leading to cell rounding (Schmidt et al., 2008). Moreover, these authors promoted the notion that MICAL1 has auto-inhibitive activity, and that binding to CRMP proteins releases this inhibition to allow the reduction in cell area to proceed (Schmidt et al., 2008). However, the mechanisms by which the MICAL1 FAD induces this reduction, and the mode by which the full-length protein is inhibitory, are not well understood. It is possible that the uninhibited MICAL1 FAD domain is so active that it dismantles the lamellipodia by completely destabilizing actin microfilaments. Similarly, the mechanism by which MICAL2 FAD overexpression, in our hands, led to an increase in actin-rich protrusions also remains to be delineated. The generation of filopodia is a complicated process that remains somewhat controversial (Faix et al., 2009), with a suite of upstream regulators including the Rho family GTPases. It might be that the dismantling of stress fibers increases the cellular pool of available actin, which is repurposed and shunted into pathways that create filopodial-like structures. Future experiments will be required to understand these interrelated processes.

In our experiments using RNA interference to deplete mammalian MICAL1 or MICAL2, we observed actin-rich protrusions of actin filaments, supporting our hypothesis that these proteins play a role in actin regulation in a non-neural context. It is interesting to note that overexpression of MICAL2 (and the FAD domains of either MICAL1 or MICAL2) induced phenotypic effects that bear similarity to those observed upon depletion of either protein, with notable loss of stress fibers and, in the case of MICAL2, generation of peripheral membrane actin-rich protrusions. Although the mechanism for this remains unknown, it is possible that knockdown of one MICAL induces compensatory action in another MICAL or one or more of its various isoforms, thus causing an overall level of enhanced ROS (as observed upon overexpression). Alternatively, it is possible that the absence of a particular MICAL alters the behavior of other actin-regulatory proteins also known to act at cytoplasmic plexin receptors, including Rho and Ras, or indeed of the GTPase-activating protein domain of plexin itself, all of which might be delicately balanced (reviewed by Hung and Terman, 2011).

Overall, our study indicates that the mammalian MICAL proteins not only play a role in semaphorin-mediated repulsive signaling in neural cells, but are also crucial regulators of actin stress fibers in non-neural cells. Actin is one of the most abundant proteins in eukaryotic cells, and plays an essential role in cell shape and survival, as well as providing the force for transport of intracellular molecules and cell movement (reviewed by Pollard and Cooper, 2009). By elucidating the specific functional roles of the mammalian MICAL family proteins in non-neural cells, our studies shed new light on the mechanisms regulating actin microfilaments.

Materials and Methods

Recombinant DNA constructs

Human *MICAL1* and *MICAL2* cDNA clones were purchased from Invitrogen (Carlsbad, CA) and cloned into a hemagglutinin fusion mammalian expression vector pHA-CMV (Clontech, Palo Alto, CA) using standard cloning procedures. MICAL1 and MICAL2 truncation mutants, FAD-dominant-negative and MICAL1 A940P, A941P mutants were generated using the QuickChange site-directed mutagenesis kit (Stratagene, La Jolla, CA). siRNA-resistant constructs of HA–MICAL1 and HA–MICAL2 were generated similarly by creating silent cDNA mutations in the oligonucleotide-binding region. The MICAL1–MICAL2 chimera was created by cloning residues 1–634 of MICAL1 and residues 611–1124 of MICAL2 into the pHA-CMV vector. Similarly, the MICAL2–MICAL1 chimera was generated by cloning residues 1–635 of MICAL2 and residues 608–1067 of MICAL1 into the pHA-CMV vector. The MICAL1 FAD domain (residues 1–500) was cloned into ptd-Tomato-C3 (Clontech) using standard cloning procedures.

Antibodies and reagents

The following antibodies were used in this study: rabbit polyclonal antibody against MICAL1 (ProteinTech, Chicago, IL); mouse monoclonal antibodies directed against the HA epitope (Covance, Princeton, NJ); mouse anti-EEA1 (BD Biosciences, San Jose, CA); mouse anti-α-tubulin (Invitrogen); mouse anti-γ-tubulin (Sigma-Aldrich); mouse anti-actin and rabbit anti-Giantin (Abcam, Cambridge, MA); rabbit anti-HA (Bethyl, Montgomery, TX); rabbit antibody against phosphorylated paxillin (Biosource, Camerillo, CA); and rat anti-Hsc70 (Stressgen, Ann Arbor, MI). The Alexa-Fluor-488-conjugated phalloidin and secondary Alexa-Fluor-568-conjugated goat anti-mouse, Alexa-Fluor-488-conjugated goat anti-mouse, and Alexa-Fluor-568-conjugated goat anti-rabbit antibodies were purchased from Invitrogen. Goat anti-mouse horseradish peroxidase (HRP) was obtained from Jackson ImmunoResearch Laboratories (West Grove, PA). Donkey anti-rabbit HRP was obtained from GE Life Sciences (Piscataway, NJ). Dihydrocalcein and *N*-acetyl cysteine were purchased from Invitrogen and Sigma (St. Louis, MO), respectively. Dihydro-dichlorofluorescein diacetate (H_2DCFDA) was kindly provided by Surinder Batra (UNMC, Omaha, NE).

Transfection and siRNA treatment

HeLa cells were transfected with plasmids using GeneExpresso DNA in vitro Transfection Reagent (Lab Supply Mall, Gaithersburg, MD) using the protocol specified by the company. On-Target SMART pool siRNA from Dharmacon (Lafayette, CO) was used to knock down MICAL1, MICAL2 and MICAL3 expression (using 300, 400 and 400 nM concentrations, respectively). siRNA knockdowns were performed as previously described (Sharma et al., 2009).

Immunofluorescence

Immunofluorescence staining was carried out as previously described (Naslavsky et al., 2006). Image acquisition and processing were performed as previously

described (Sharma et al., 2009), using a Zeiss LSM5 Pascal confocal microscope with a 63× objective (numerical aperture 1.4).

Reactive oxygen species measurements

HeLa cells grown on coverslips or Lab-Tek chambered coverglass systems (Nunc, Rochester, NY) were either transfected or left untransfected. After 18 hours, cells were either fixed or washed and incubated with 10 μM dihydrocalcein or H_2DCFDA dissolved in DMEM (without Phenol Red, which interferes with the ROS measurements) for 30 minutes at 37℃. Dihydrocalcein- or H_2DCFDA-treated cells were then washed and incubated with DMEM containing 10% fetal bovine serum (but lacking Phenol Red). After 10 minutes, cells were imaged by confocal microscopy with a 10× objective. Manual counting was performed on dihydrocalcein-treated cells to calculate the number and ratio of fluorescent (ROS-containing) cells in each case. In parallel, fixed cells were washed, permeabilized and incubated with anti-HA followed by Alexa-Fluor-568-conjugated anti-mouse antibody. Cells were then mounted with solution containing DAPI. Images were obtained to quantify the transfection ratio. ROS levels were calculated from the ratio of cells fluorescing upon dihydrocalcein treatment divided by the overall transfection ratio. Experiments were performed three times and standard errors were determined.

Reverse transcriptase PCR

Hela cells were grown on 35-mm dishes to ~90% confluency. mRNA from HeLa cells was extracted using RNeasy Mini Kit (Qiagen). cDNA was then prepared from HeLa mRNA using SuperScript III First-strand Synthesis System for RT-PCR (Invitrogen). PCR reactions were performed with pfuTurbo DNA polymerase (Agilent, Santa Clara, CA). Primers for RT-PCR that are specific for β-actin, MICAL1, MICAL2 and MICAL3 were designed using primer blast. The primers used for actin were 5′-CCTCGCCTTTGCCGATCC-3′ and 5′-GGATCTTCA-TGAGGTAGTCAGTC-3′. The primers used for MICAL1 were 5′-TGCTGGG-ACTGGTGGGGGAC-3′ and 5′-GCCGGTACACCAGGGCACAC-3′. The primer pairs that were used for MICAL2 were 5′-CACCACTGCCGCACACGACT-3′, 5′-AGTGCGCAAGCCACAGGGTC-3′; 5′-CCAAGACAACCTGCTATCCTAT-GC-3′, 5′-GTGCTCCAGCTCCTTAGTGATATAC-3′; 5′-GCCCGTGGATTCT-TGGCGCA-3′, 5′-GTGCCCCGTCACGACCACAG-3′; and 5′-CGCAGGCTCT-TTCCGGGGTG-3′, 5′-CACGTGTCGCTGCCTCCCAG-3′. The primer pairs 5′-ATCGGCATACGGAGACAGGGCTC-3′, 5′-ATCTCCAGAGGATCCGCCGC-G->3′ and 5′-AGAGAACCCCAGGTTCAGGCGT-3′, 5′-TCTTCCCCTCACAA-CGCACTTGCT-3′ were used for MICAL3 isoform1 and isoform3, respectively.

Acknowledgements

The authors gratefully acknowledge the assistance of Subhankar Chakraborty and Srustidhar Das for their assistance with the reverse transcriptase PCR experiments.

Funding

This research was supported by National Institutes of Health [grant numbers RO1GM074876, RO1GM087455 to S.C. and N.N.], the National Center for Research Resources [grant number P20 RRO18759 to N.N.], a University of Nebraska Student Assistantship Award (to S.S.P.G.) and the Welcome Trust (to J.R.). Deposited in PMC for release after 6 months.

Supplementary material available online at
http://jcs.biologists.org/lookup/suppl/doi:10.1242/jcs.089367/-/DC1

References

Ashida, S., Furihata, M., Katagiri, T., Tamura, K., Anazawa, Y., Yoshioka, H., Miki, T., Fujioka, T., Shuin, T., Nakamura, Y. et al. (2006). Expression of novel molecules, MICAL2-PV (MICAL2 prostate cancer variants), increases with high Gleason score and prostate cancer progression. *Clin. Cancer Res.* **12**, 2767-2773.

Beuchle, D., Schwarz, H., Langegger, M., Koch, I. and Aberle, H. (2007). Drosophila MICAL regulates myofilament organization and synaptic structure. *Mech. Dev.* **124**, 390-406.

Bron, R., Vermeren, M., Kokot, N., Andrews, W., Little, G. E., Mitchell, K. J. and Cohen, J. (2007). Boundary cap cells constrain spinal motor neuron somal migration at motor exit points by a semaphorin-plexin mechanism. *Neural Dev.* **2**, 21.

Dalle-Donne, I., Rossi, R., Giustarini, D., Gagliano, N., Di Simplicio, P., Colombo, R. and Milzani, A. (2002). Methionine oxidation as a major cause of the functional impairment of oxidized actin. *Free Radic. Biol. Med.* **32**, 927-937.

Faix, J., Breitsprecher, D., Stradal, T. E. and Rottner, K. (2009). Filopodia: complex models for simple rods. *Int. J. Biochem. Cell Biol.* **41**, 1656-1664.

Fedorova, M., Kuleva, N. and Hoffmann, R. (2010). Identification of cysteine, methionine and tryptophan residues of actin oxidized in vivo during oxidative stress. *J. Proteome Res.* **9**, 1598-1609.

Grigoriev, I., Yu, K. L., Martinez-Sanchez, E., Serra-Marques, A., Smal, I., Meijering, E., Demmers, J., Peranen, J., Pasterkamp, R. J., van der Sluijs, P. et al. (2011). Rab6, Rab8, and MICAL3 cooperate in controlling docking and fusion of exocytotic carriers. *Curr. Biol.* **21**, 967-974.

He, Z., Wang, K. C., Koprivica, V., Ming, G. and Song, H. J. (2002). Knowing how to navigate: mechanisms of semaphorin signaling in the nervous system. *Sci. STKE* **2002**, re1.

Hung, R. J. and Terman, J. R. (2011). Extracellular inhibitors repellents and semaphorin/plexin/MICAL-mediated actin filament disassembly. *Cytoskeleton (Hoboken)* **68**, 415-433.

Hung, R. J., Yazdani, U., Yoon, J., Wu, H., Yang, T., Gupta, N., Huang, Z., van Berkel, W. J. and Terman, J. R. (2010). Mical links semaphorins to F-actin disassembly. *Nature* **463**, 823-827.

Kalil, K. and Dent, E. W. (2005). Touch and go: guidance cues signal to the growth cone cytoskeleton. *Curr. Opin. Neurobiol.* **15**, 521-526.

Kirilly, D., Gu, Y., Huang, Y., Wu, Z., Bashirullah, A., Low, B. C., Kolodkin, A. L., Wang, H. and Yu, F. (2009). A genetic pathway composed of Sox14 and Mical governs severing of dendrites during pruning. *Nat. Neurosci.* **12**, 1497-1505.

Kolk, S. M. and Pasterkamp, R. J. (2007). MICAL flavoprotein monooxygenases: structure, function and role in semaphorin signaling. *Adv. Exp. Med. Biol.* **600**, 38-51.

Moldovan, L., Irani, K., Moldovan, N. I., Finkel, T. and Goldschmidt-Clermont, P. J. (1999). The actin cytoskeleton reorganization induced by Rac1 requires the production of superoxide. *Antioxid. Redox Signal.* **1**, 29-43.

Nadella, M., Bianchet, M. A., Gabelli, S. B., Barrila, J. and Amzel, L. M. (2005). Structure and activity of the axon guidance protein MICAL. *Proc. Natl. Acad. Sci. USA* **102**, 16830-16835.

Naslavsky, N., Rahajeng, J., Sharma, M., Jovic, M. and Caplan, S. (2006). Interactions between EHD proteins and Rab11-FIP2: a role for EHD3 in early endosomal transport. *Mol. Biol. Cell* **17**, 163-177.

Nimnual, A. S., Taylor, L. J. and Bar-Sagi, D. (2003). Redox-dependent down-regulation of Rho by Rac. *Nat. Cell Biol.* **5**, 236-241.

Pak, C. W., Flynn, K. C. and Bamburg, J. R. (2008). Actin-binding proteins take the reins in growth cones. *Nat. Rev. Neurosci.* **9**, 136-147.

Pasterkamp, R. J., Dai, H. N., Terman, J. R., Wahlin, K. J., Kim, B., Bregman, B. S., Popovich, P. G. and Kolodkin, A. L. (2006). MICAL flavoprotein monooxygenases: expression during neural development and following spinal cord injuries in the rat. *Mol. Cell Neurosci.* **31**, 52-69.

Pollard, T. D. and Cooper, J. A. (2009). Actin, a central player in cell shape and movement. *Science* **326**, 1208-1212.

Raper, J. A. (2000). Semaphorins and their receptors in vertebrates and invertebrates. *Curr. Opin. Neurobiol.* **10**, 88-94.

Ridley, A. J. and Hall, A. (1992). The small GTP-binding protein rho regulates the assembly of focal adhesions and actin stress fibers in response to growth factors. *Cell* **70**, 389-399.

Schmidt, E. F., Shim, S. O. and Strittmatter, S. M. (2008). Release of MICAL autoinhibition by semaphorin-plexin signaling promotes interaction with collapsin response mediator protein. *J. Neurosci.* **28**, 2287-2297.

Sharma, M., Giridharan, S. S., Rahajeng, J., Naslavsky, N. and Caplan, S. (2009). MICAL-L1 links EHD1 to tubular recycling endosomes and regulates receptor recycling. *Mol. Biol. Cell* **20**, 5181-5194.

Sutherland, J. D. and Witke, W. (1999). Molecular genetic approaches to understanding the actin cytoskeleton. *Curr. Opin. Cell Biol.* **11**, 142-151.

Suzuki, T., Nakamoto, T., Ogawa, S., Seo, S., Matsumura, T., Tachibana, K., Morimoto, C. and Hirai, H. (2002). MICAL, a novel CasL interacting molecule, associates with vimentin. *J. Biol. Chem.* **277**, 14933-14941.

Terai, T., Nishimura, N., Kanda, I., Yasui, N. and Sasaki, T. (2006). JRAB/MICAL-L2 is a junctional Rab13-binding protein mediating the endocytic recycling of occludin. *Mol. Biol. Cell* **17**, 2465-2475.

Terman, J. R., Mao, T., Pasterkamp, R. J., Yu, H. H. and Kolodkin, A. L. (2002). MICALs, a family of conserved flavoprotein oxidoreductases, function in plexin-mediated axonal repulsion. *Cell* **109**, 887-900.

Weide, T., Teuber, J., Bayer, M. and Barnekow, A. (2003). MICAL-1 isoforms, novel rab1 interacting proteins. *Biochem. Biophys. Res. Commun.* **306**, 79-86.

Yu, H. H., Araj, H. H., Ralls, S. A. and Kolodkin, A. L. (1998). The transmembrane Semaphorin Sema I is required in Drosophila for embryonic motor and CNS axon guidance. *Neuron* **20**, 207-220.

Zhou, Y., Adolfs, Y., Pijnappel, W. W., Fuller, S. J., van der Schors, R. C., Li, K. W., Sugden, P. H., Smit, A. B., Hergovich, A. and Pasterkamp, R. J. (2011b). MICAL-1 is a Negative Regulator of MST-NDR Kinase Signaling and Apoptosis. *Mol. Cell Biol.* **31**, 3603-3615.

Zhou, Y., Gunput, R. A., Adolfs, Y. and Pasterkamp, R. J. (2011a). MICALs in control of the cytoskeleton exocytosis and cell death. *Cell Mol. Life Sci.* **68**, 4033-4044.

Zucchini, D., Caprini, G., Pasterkamp, R. J., Tedeschi, G. and Vanoni, M. A. (2011). Kinetic and spectroscopic characterization of the putative monooxygenase domain of human MICAL-1. *Arch. Biochem. Biophys.* **515**, 1-13.

Supplementary Fig. 1

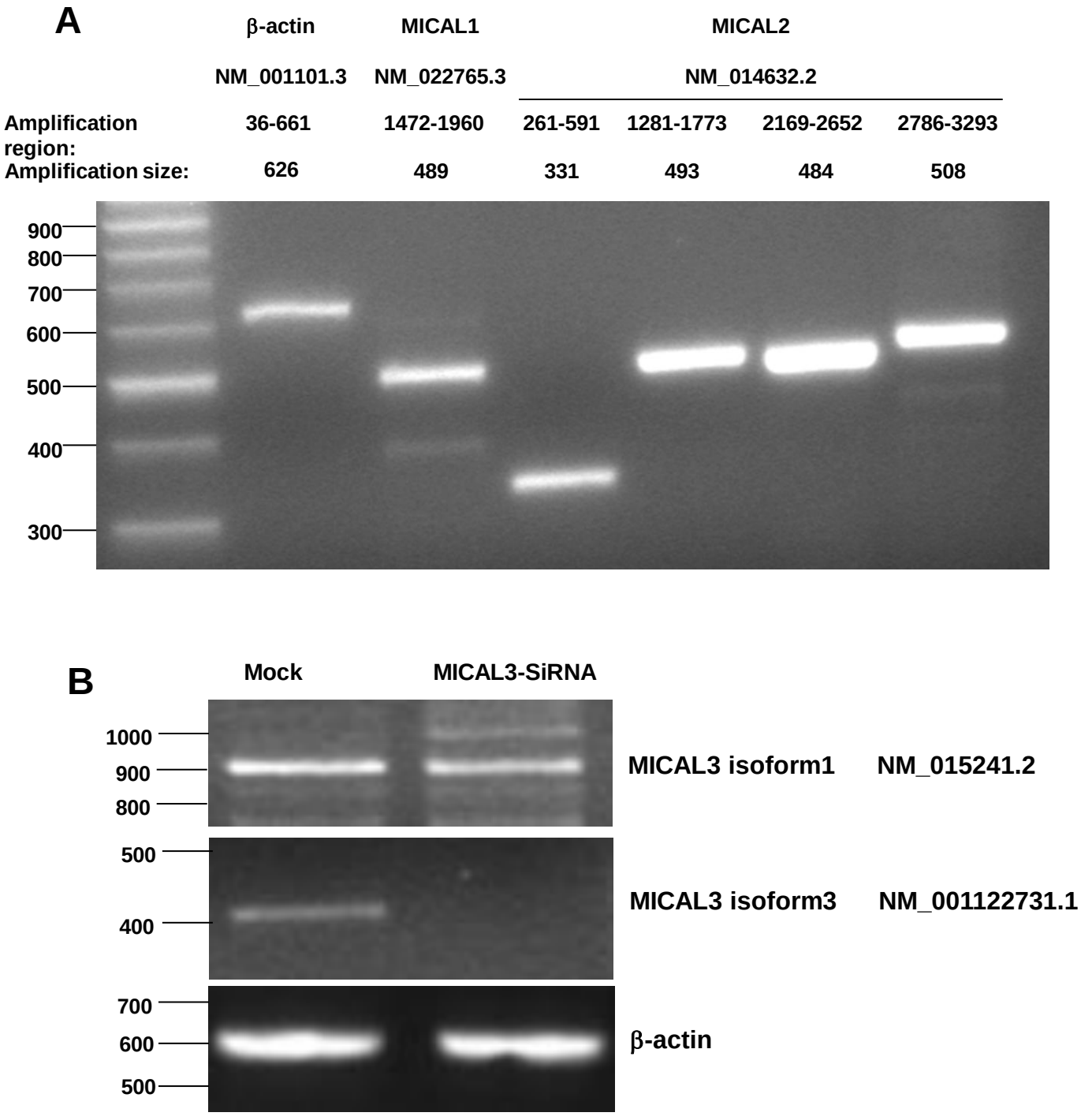

Supplementary Fig.2

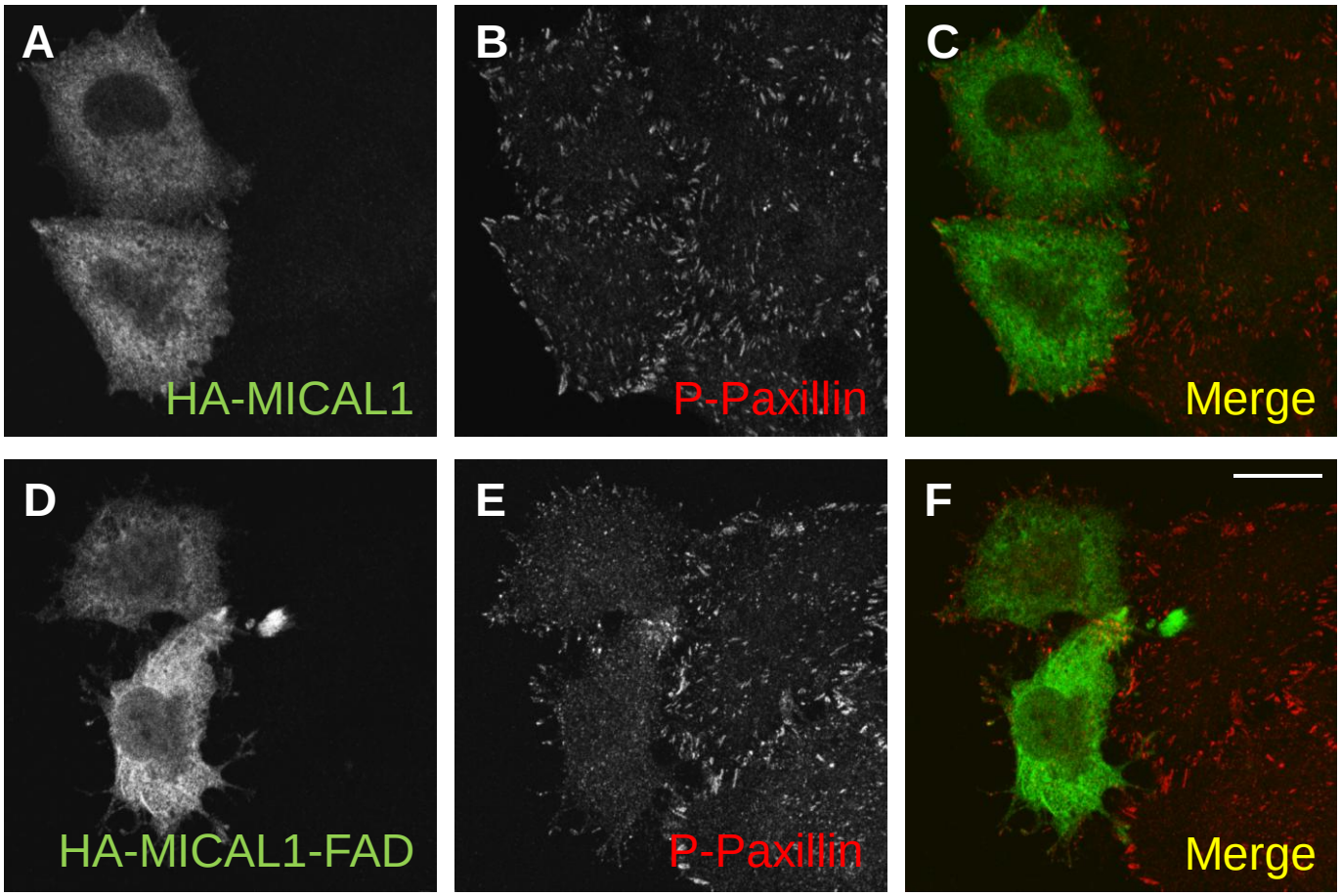

Supplementary Fig. 3

A

MICAL1 CC domain (925-961 residues):

FCKAQTIQRRLNEIE**AA**LRELEAEGVKLELALRRQSS

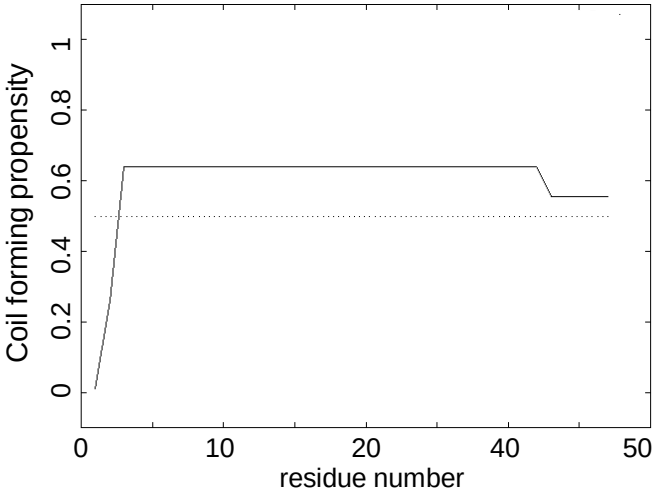

B

MICAL1 CC domain (925-961 residues) A940P, A941P:

FCKAQTIQRRLNEIE**PP**LRELEAEGVKLELALRRQSS

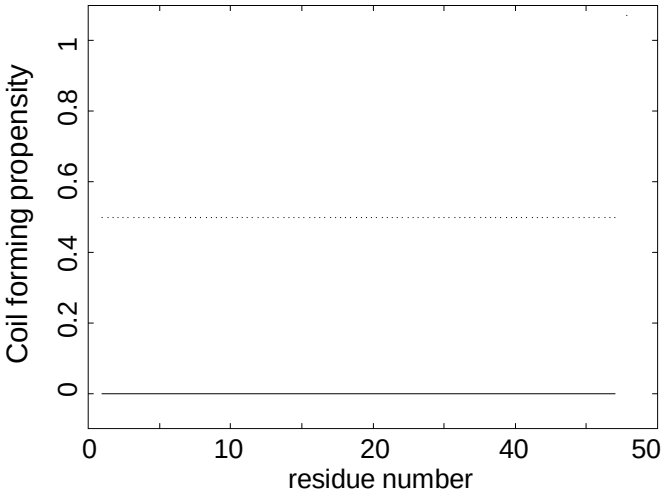

Supplementary Fig. 4

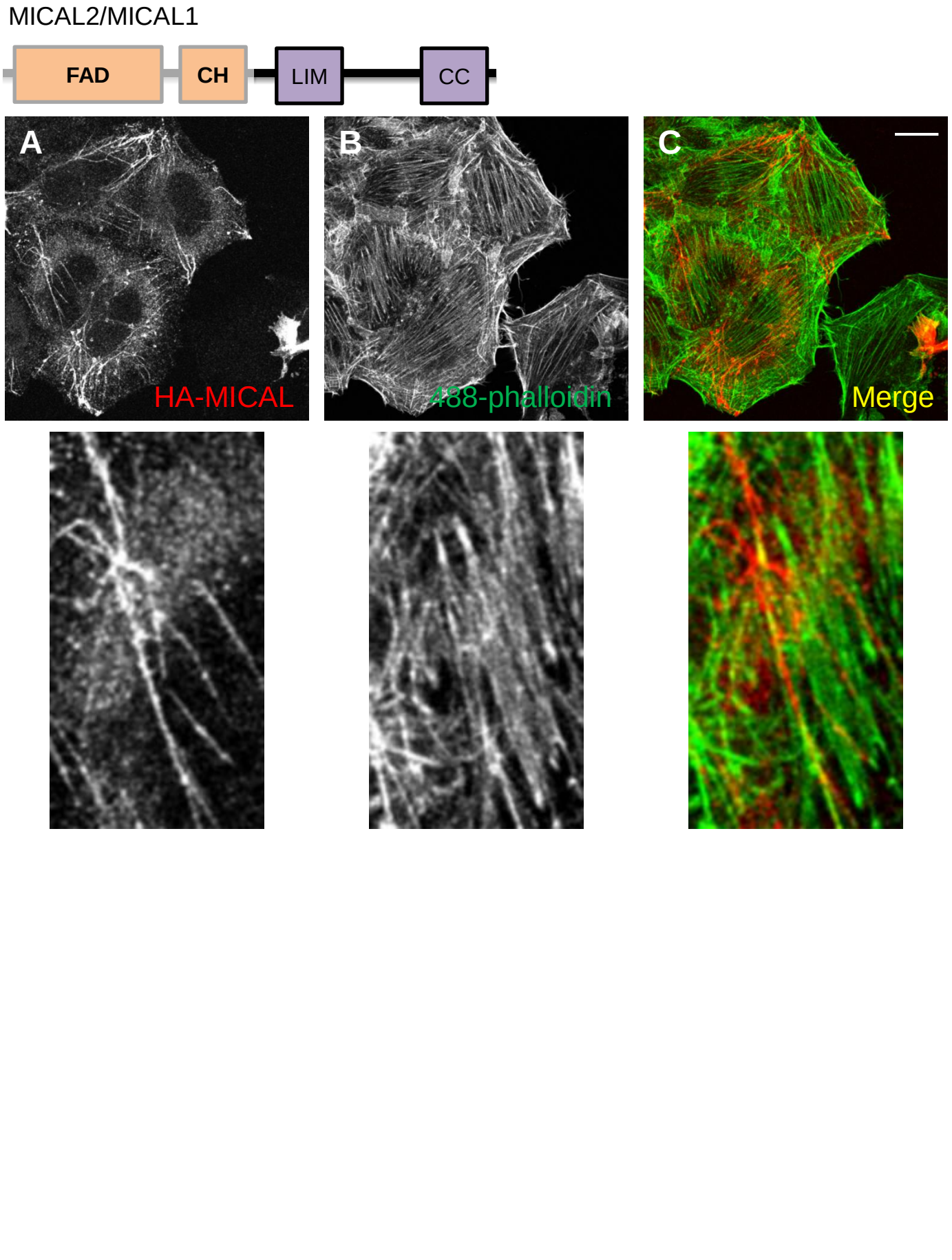

Supplementary Fig. 5A

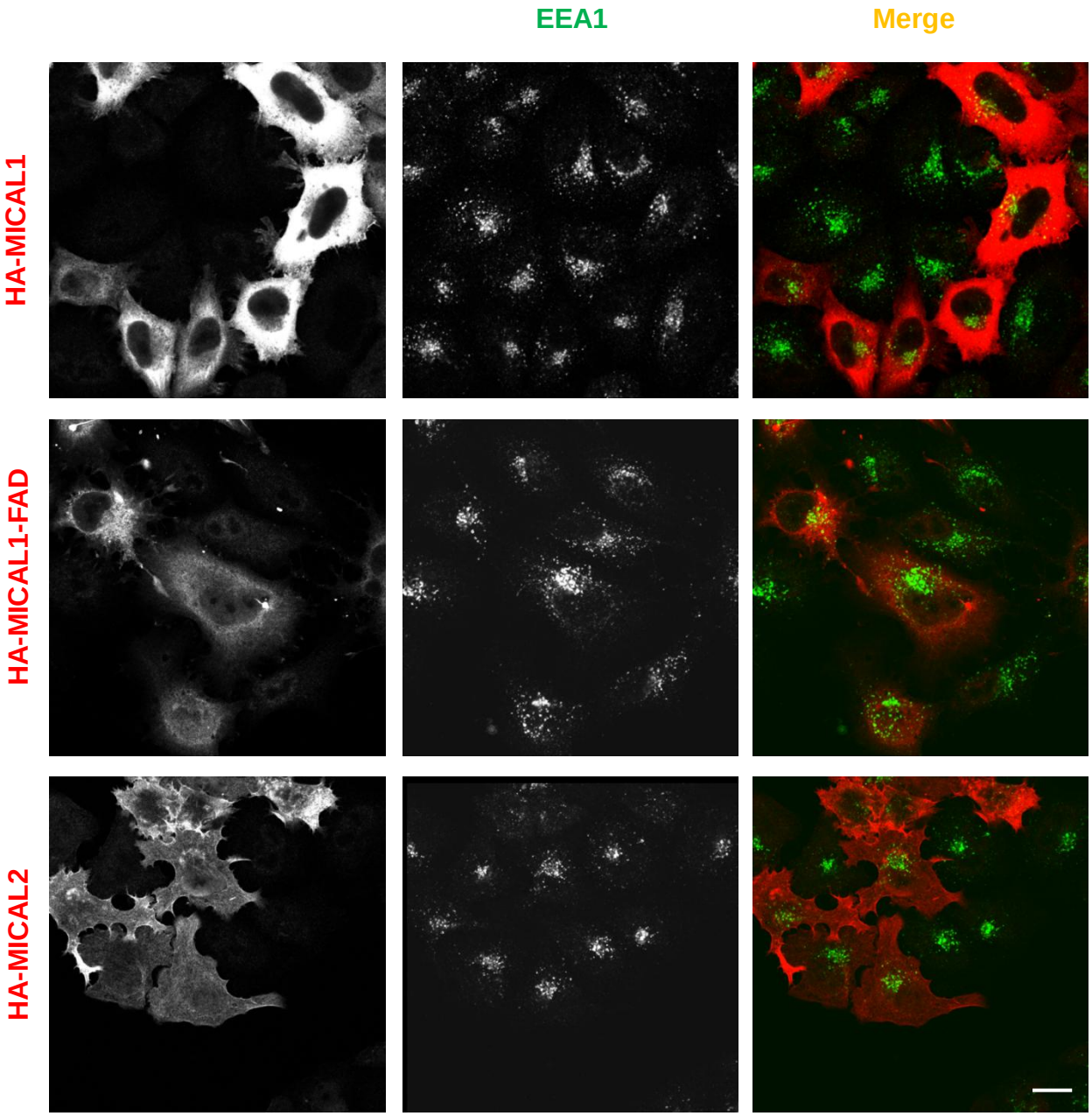

Supplementary Fig. 5B

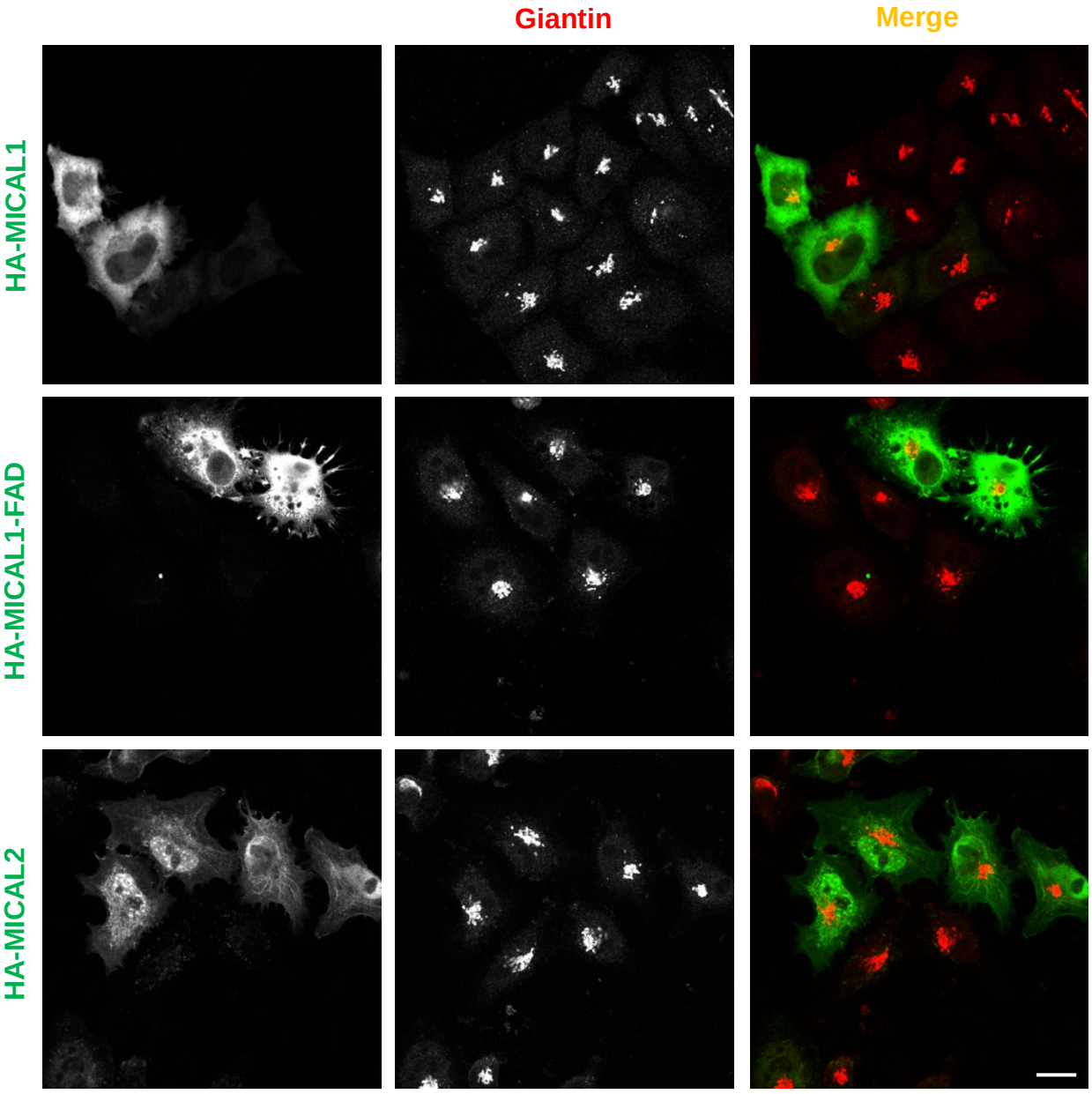

Supplementary Fig. 5C

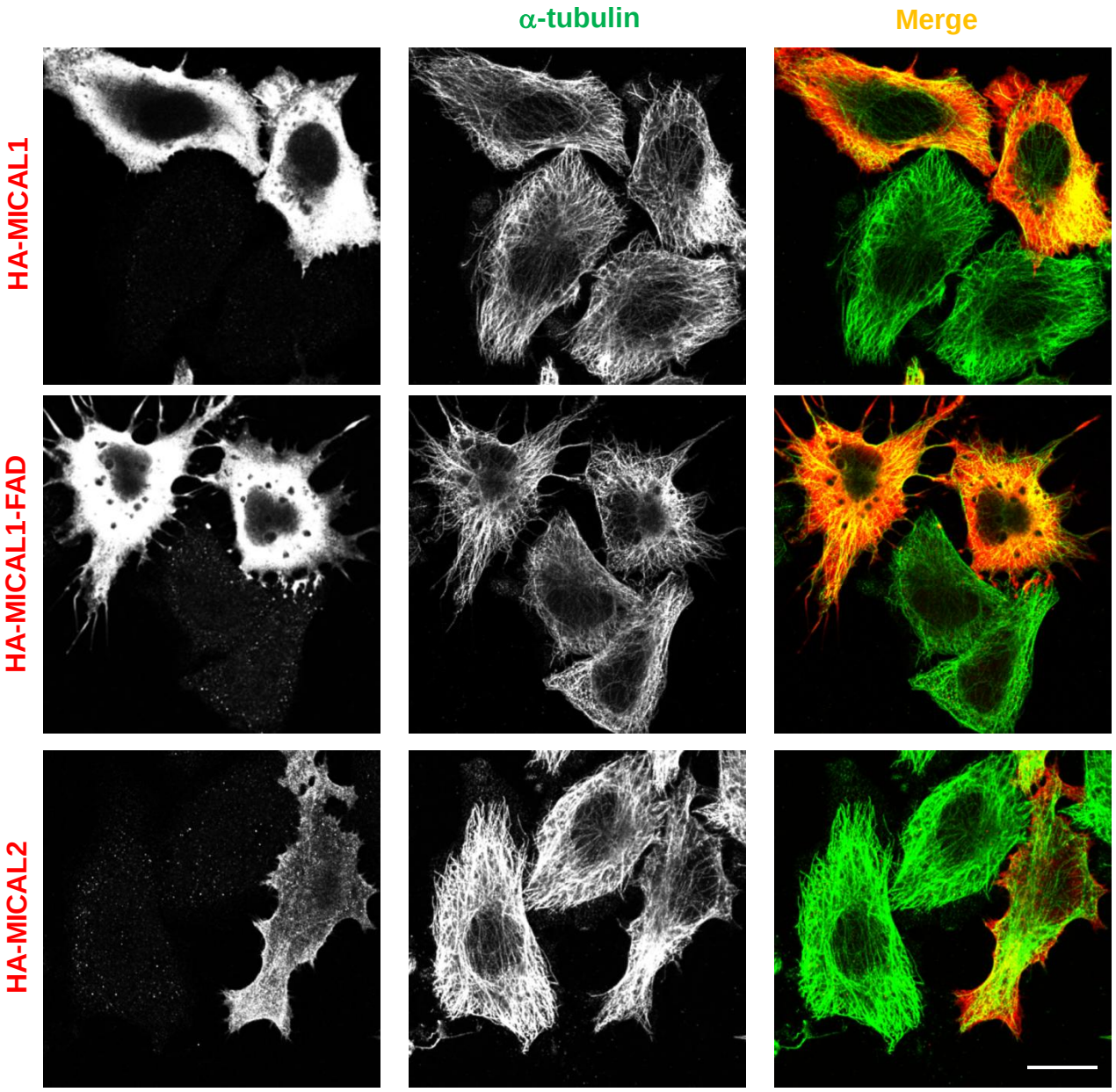

Supplementary Fig. 5D

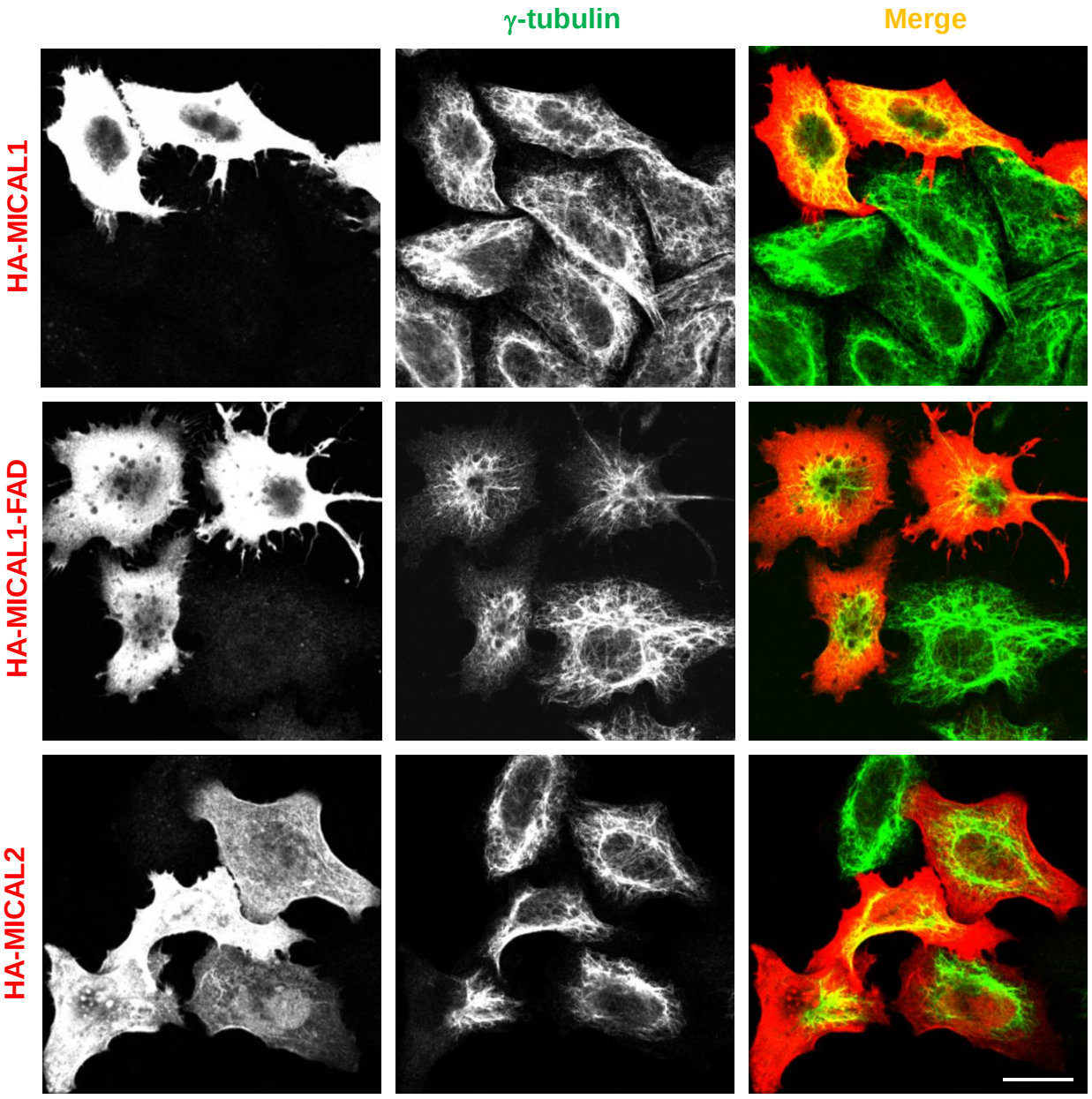

Supplementary Fig. 6

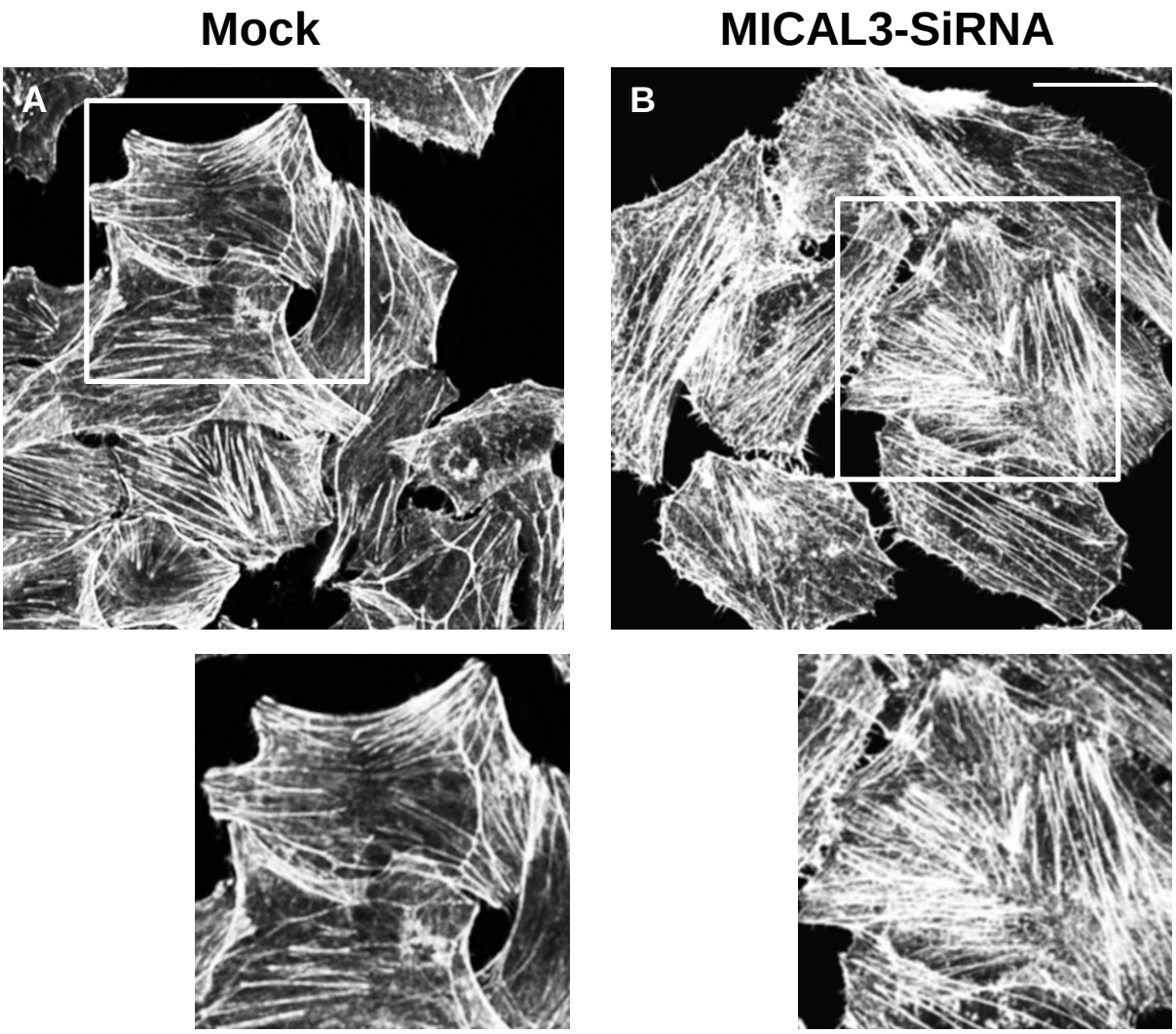

Supplementary Fig. 7